Ternary Polymer Solutions Studied By Dynamic Light Scattering and Ultracentrifugation

A thesis presented in partial fulfilment
of the requirements for the degree of

Master of Science in Physics

at

Massey University
New Zealand

Tu'ivaita Ueleni
1996

DEDICATION

To my mother, Veisinia Ueleni; my sisters and brothers and to my Church, "Siasi Tokaikolo 'Ia Kalaisi".

ABSTRACT

Dynamic light scattering has been used to measure the interpenetration diffusion coefficient of ternary polymer solutions formed with 233 000 dalton polystyrene and a trace amount of 330 000 dalton PMMA dissolved in thiophenol. These measurements have been compared with the diffusion coefficients obtained from ultracentrifuge studies of the same solutions by observing the change in shape of the sedimentation boundary curve with time.

This novel use of ultra centrifugation to measure diffusion coefficients in ternary polymer solutions is possible because; (i) the solvent is isorefractive and isopycnic with polystyrene, and (ii) the PMMA was the minority polymer in the solutions studied (concentration 0.001 g/g). Hence only the PMMA was visible and it sedimented through an effective solvent of thiophenol and polystyrene. All measurements were made at 25°C.

The diffusion coefficients obtained from the ultracentrifuge observations are in good agreement with the interpenetration diffusion coefficients obtained from dynamic light scattering studies on the same solutions. Solutions formed at polymer concentrations greater than 0.1 g/g suffered phase separation since PMMA and polystyrene are incompatible polymers. The solution with polymer concentration 0.0755 g/g was too unstable for ultra centrifugation studies, but was susceptible to investigation by dynamic light scattering. The interpenetration diffusion coefficient of this solution was found to be much smaller than those of the more dilute solutions.

The temperature dependence of the interpenetration diffusion coefficient was also investigated on the solution with the largest polymer concentration. The interpenetration diffusion coefficient was found to decrease as the temperature was lowered. This behaviour is consistent with the prediction that the interpenetration diffusion coefficient approaches zero as phase separation is approached. A value for correlation length critical exponent, n, of this ternary solution system was found. This is the first time that dynamic light scattering has been used (successfully) to obtain a value for n.

Dynamic light scattering and ultra centrifugation were also used to investigate the dynamical behaviour of ternary polymer solutions formed with 233 000 dalton polystyrene and a trace amount of 110 000 dalton poly(vinyl methyl ether) (PVME) dissolved in thiophenol. The preparation of this PVME fraction is described here. The fractionation was achieved by batch fractional precipitation from toluene solution with petroleum spirit.

All ultra centrifugation studies carried out on this system were unsuccessful because the solutions phase separated when subjected to strong centrifugal forces. The results of the light scattering measurements are reported and discussed.

ACKNOWLEDGMENTS

First and foremost, I would like to thank my supervisors, Assoc. Prof. Neil Pinder and Dr. Jim Lewis for their valuable guidance, advice and encouragement throughout this project.

I am grateful for the support and friendly environment provided by the staff of the Physics Department at Massey University.

I also wish to thank those who instructed me in the use of various items of specialised apparatus in both the Physics and Chemistry Departments. Dr. Yi Luo deserves special mention for guiding me through most of the computer software used for writing up this thesis.

I would also like to thank the president of my church, Dr. Liufau Vailea Saulala, for his encouragement, vision and prayers and also for giving me this opportunity to complete this degree. Many thanks are also given to Rev. Sione Finau and the church members in New Zealand for their kindness, prayers and financial support throughout this course.

Finally, by no means the least, I wish to thank all those who provided me with support and encouragement throughout this thesis but their names are not mentioned above.

TABLE OF CONTENTS

LIST OF FIGURES

LISTS OF TABLES

Chapter 1
Introduction

There is great interest in polymer mixtures since it is widely believed that important new polymer materials are likely to be developed from mixtures of known polymers rather than from entirely new ones. This interest in polymer mixtures has in turn stimulated interest in polymer ternary solutions, that is solutions formed from two dissimilar mono disperse random coil polymers dissolved in a low molar mass solvent. The dynamical behaviour of these ternary solutions must be thoroughly understood if stable composite polymer materials are to be developed.

The interaction between polymers is described by the Flory-Huggings interaction parameter χ, which is positive for dissimilar polymers that do not intermix in the melt (but which instead form two separate phases). However if such polymers are dissolved in a suitable low molar mass solvent then single phased solutions can be stable in certain composition, concentration and temperature regimes thus promoting polymer mixing and enabling the parameter χ to be determined. The theoretical development has assumed χ, to be constant for any given pair of polymers and that the compatibility of the two polymers is governed solely by χ. However the theory is known to be incomplete for χ is introduced as a constant independent of polymer composition, solvent or temperature which is contrary to experiment [43, 44]. Indeed Saeki et al [41] and Robard et al [39] have separately shown that the compatibility of two polymers in a ternary solution depends on the solvent, even polymers with a negative χ value can form two phased solutions if the solvent has sufficiently dissimilar affinities for the two polymers, thereby implying that the effective polymer-polymer interaction parameter for two polymers is solvent dependent. Nevertheless χ has proved to be a valuable yardstick for describing the thermodynamic behaviour of polymers in combination. The polymer-solvent interactions are described by the single parameter υ, the excluded volume parameter which describes the swelling of the random coils due to the finite volume of the polymer monomers.

A convenient measure of the dynamical behaviour of stable polymer ternary solutions can be obtained by considering their transport parameter coefficients. There are many diffusion coefficients which can be defined for a polymer ternary solution but only a few of which are amenable to measurement. These are the self diffusion coefficients of each of the polymers D_{S1} and D_{S2}, the self diffusion coefficient of the solvent, the

interpenetration diffusion coefficient D_I, and the cooperative diffusion coefficient D_C. It is important that these diffusion coefficients be clearly distinguished and that their properties and means of determination be appreciated.

In general there are three self diffusion coefficients in a ternary solution one for each constituent. These describe the motion of a labelled molecule in the solution in the absence of concentration gradients. The interpenetration diffusion coefficient describes the relative motion of the polymers when the total polymer concentration is constant but the relative polymer abundance varies. The cooperative diffusion coefficient describes the combined motion of both polymers under the influence of a total polymer concentration gradient, the relative abundance of the polymers being constant. Pulsed field gradient nuclear magnetic resonance (pfgnmr) can be used to measure the self diffusion coefficients of the constituents of a ternary solution providing two conditions are met. Each constituent must have a magnetic resonance which is sufficiently resolved in the frequency domain, and the concentration of the constituent must be sufficiently high for the collection of adequate data. Dynamic light scattering (dls) can be used to measure the interpenetration and cooperative diffusion coefficients to very small polymer concentrations, in addition dls observations on binary polymer solutions can be used to measure the mutual diffusion coefficient of the solution. The pfgnmr technique is far less sensitive than the dls technique so substantially larger concentrations are required, this usually means that the self diffusion coefficient of the minority polymer cannot be measured at small values of the relative abundance parameter. Nevertheless pfgnmr has provided valuable data for the experimental investigations of ternary polymer solutions because this technique always measures the self diffusion coefficient which is a precisely defined readily identifiable quantity.

Nemoto et al [30] have shown that under special circumstances ultracentrifugution can be used to measure the sedimentation coefficient of one of the polymers in a ternary polymer solution. The majority polymer and the solvent must be isorefractive and also isopycnic so that the sedimentation coefficient of the minority polymer can be obtained. The sedimentation coefficient, s, is a measure of the velocity of the sedimenting polymer molecules with respect to the high centrifugal forces involved in this technique. This technique can also be used to obtain a diffusion coefficient for ternary solutions which meets the special condition described above. A ternary system previously studied by Nemoto et al [30] was PMMA dissolved with polystyrene in thiophenol. This system was chosen because the majority polymer (polystyrene) and thiophenol were not only isorefractive but also isopycnic thus constituting an "effective solvent" through which PMMA sedimented and diffused. The system chosen for the study reported here approximated a system studied by Nemoto et al [30]. Dynamic light

scattering was used to measure the interpenetration diffusion coefficient, D_I, and ultra centrifugation was used to measure the sedimentation coefficient, s, and also a diffusion coefficient of the polymers.

This work has three principle aims:

1. To investigate the proposition that the diffusion coefficient obtained from ultracetrifugation studies of such a solution is the interpenetration diffusion coefficient obtained from dynamic light scattering studies.

2. To investigate the temperature dependence of D_I for the most concentrated sample of the ternary solution. Phase separation occurs as the temperature is lowered to the critical temperature and D_I is expected to diverge since D_I is inversely proportional to the correlation length which increases without limit as phase separation is approached.

3. To investigate the dynamical behaviour of a ternary system of PVME dissolved with polystyrene in thiophenol.

Chapter 2
Theory

2.1 Dynamic Light Scattering

The Borsali-Benmouna theory describes dynamic light scattering from semi-dilute ternary solutions of random coil polymers dissolved in an "equally good" solvent [2, 3, 5, 8]. This theory makes a number of simplifying assumptions, including the adoption of a naive Flory theory of polymer interaction so the theory is restricted to solvents which are equally good for the polymers. This implies that the polymers have equal excluded volume parameters υ. The value of υ is 0.5 for the so-called ideal polymer molecules having zero volume (these are the theoretical constraints in which the polymer is able to cross its own path). υ adopts values in the range 0.5 - 0.7 for real polymer molecules and describes the swelling of the random coil molecule due to the finite volume occupied by monomers of the real polymer molecule. The application of the Flory-Huggins theory to ternary polymer solutions is discussed by Ould Kaddour and Strazielle [26], the polymer-polymer interaction is described by the quantity χ which is assumed to depend on the polymers only, in particular χ is assumed to be independent of the solution composition, concentration or temperature and the quality of the solvent. The use of the random phase approximation together with the assumption that hydrodynamic interactions are totally screened limits the application of the Benoit-Benmouna theory to polymer concentrations less than the entanglement concentration but greater than the overlap concentration c^*. The solution must also be sufficiently far from the spinodal as is discussed by Benmouna et al [2].

2.1(a). The Diffusion Coefficients

Pusey et al. [38] discussed dynamic light scattering from ternary solutions and were able to show that the field autocorrelation function exhibited two decay processes and was given by

$$g^1(\tau) = A_+ \exp(-D_+ q^2 \tau) + A_- \exp(-D_- q^2 \tau) \qquad (2.1)$$

The + mode is the cooperative mode and describes the decay of the total polymer concentration $(\delta c_1 + \delta c_2)$ at constant polymer relative abundance, $[\delta(c_1 / c_2)$ is zero$]$. The - mode is the interpenetration mode and describes fluctuations in the relative abundance of the polymers at constant total polymer concentration $[(\delta c_1 + \delta c_2)$ is zero$]$. The cooperative

mode governs the fast decay and the interpenetration mode governs the slow decay. These decay rates, Γ_- and Γ_+ respectively can be measured to determine the corresponding diffusion coefficients.

Benmouna et al [2] obtained an expression for the initial slope of the natural logarithm of the dynamic structure facture, and hence predicted that the field auto correlation function of the scattered light should be composed of just two decays. A simplified version of the theory is presented here since the work to be presented is concerned with polymers whose molar masses are less than 500 000 daltons, and the particle form factors as taken as unity. For the special case of polymers with equal degrees of polymerisation

$$\Gamma_I/q^2 = D_I = D_{S2}[1-2\phi\chi Nx(1-x)] \tag{2.2}$$

$$\Gamma_C/q^2 = D_C = D_{S2}[1-\upsilon\phi N] \tag{2.3}$$

Appealing to the "identification"

$$\upsilon\phi N = 2cMA_2 \tag{2.4}$$

the expression for D_I can be written as

$$D_I = D_{S2}[1-4A_2Mcx(1-x)\chi/\upsilon] \tag{2.5}$$

where υ is the excluded volume parameter, c is the total polymer concentration in g.ml^{-1}, M is the polymer molar mass, and x the polymer relative abundance parameter given by the concentration of polymer 1 divided by c. Notice the diffusion coefficients D_C and D_I are identified with the cooperative and interpenetration diffusion coefficients D_+ and D_- respectively.

Rouse dynamics are assumed in this theory so the self diffusion coefficient of polymer 2, D_{S2} is taken as $k_BT/N\zeta$, where ζ is the friction factor per monomer. Note N is the degree of polymerisation, that is $M = Nm$, where m is the monomer molar mass.
The self diffusion coefficient of polymer 2 (usually the majority polymer), in the ternary solution is distinct from the self diffusion coefficient of the same polymer in a binary solution of the same concentration. Polymer-polymer interaction is described by χ/υ in this theory. A cautionary note should be added here, A_2 and χ/υ are expected to be concentration dependent. Indeed Daoud renormalised υ as a function of c, and the des Cloizeaux law for osmotic pressure implies that A_2 scales as $c^{0.25}$ in the semi dilute regime (Benoit and Benmouna (1984) [4].

For unequal molar mass polymers the expressions for D_C and D_I become

$$D_C, D_I = D_{S2}[A \pm 0.5\sqrt{F - E + G}] \tag{2.6}$$

where

$$A = 0.5[N_2/N_1 + 1 + \upsilon\phi N_2],$$

$$E = -4x\upsilon\phi N_2(1 - N_2/N_1),$$

$$F = 8x(1-x)(\upsilon\phi N_2)^2\,\chi/\upsilon$$

$$G = 4(A - N_2/N_1)^2$$

In the above, ϕ is the polymer volume fraction, N_1 and N_2 are the degrees of polymerisation of polymers 1 and 2, and υ and χ are the polymer excluded volume and polymer-polymer interaction parameters, respectively. The E and F terms can be identified with the effects of unequal degrees of polymerisation, and polymer incompatibility respectively.

Some trivial though important observations should be made at this point. Firstly, the decay rates do not contain information regarding the optical properties of the solvent or solutes, so the decay rates and associated diffusion coefficients are independent of the optical properties of the solution. Secondly, the interpenetration diffusion coefficient differs from the self diffusion coefficient of polymer 2 in the ternary solution, unless the polymers are compatible and have equal degrees of polymerisation. In general these two diffusion coefficients are distinct, the difference between the two increases as the degree of polymerisation ratio increases particularly if $N_2 < N_1$. The difference also depends on the polymer relative abundance parameter x and the total polymer concentration c. The difference between these two diffusion coefficients also depends on the compatibility of the polymers. This has excited some interest, however, it should be appreciated that the incompatibility factor can be significant only close to the spinodal or if the degrees of polymerisation are nearly equal.

The theory is known to have some deficiencies. First, the theory contains some delicate points, not only does it identify D_C and D_I with D_+ and D_- respectively but it also make use of another "identifications"

$$\upsilon\phi N = 2cMA_2 = 2c/c^* \tag{2.7}$$

Where c and c^* are the total polymer concentration and the overlap concentration respectively (in g.ml^{-1}), ϕ is the polymer volume fraction, M the polymer molar mass, N the degree of polymerisation, and A_2 is the second viral coefficient. These are not essential structures of the Benoit-Benmouna theory [4], they merely facilitate comparison between theory and experiment. Secondly, although the theory predicts D_I to vanish as phase separation is approached, there are ambiguities and the theory is considered to be inadequate close to phase separation.

2.1(b). Diffusion Close to Phase Separation

Although the simple Benmouna theory ignores the so-called memory effects and only partially accounts for hydrodynamic interactions, the theory is able to provide an adequate account of the behaviour of ternary polymer solutions far from phase separation where the effects of hydrodynamic interactions are negligible. However ternary solutions close to phase separation are characterised by the correlation length (ξ) diverging so long range hydrodynamic effects are significant in the critical region where ξ varies with temperature as :

$$\xi \propto \left\{(T_C - T)/T\right\}^{-n} \tag{2.8}$$

where T and T_C are the temperature and the critical temperature of the solution. The mean field theory, the three dimensional Ising and the Fisher renormalisation values for the critical exponent n are 0.5, 0.63 and 0.71 respectively.

Benmouna et al [4] have extended the simple theory to include hydrodynamic interactions for the symmetric case in which the polymers have equal degrees of polymerisation, equal monomer friction coefficients, equal and opposite refractive index increments and equal concentrations. They found that only the interpenetration mode was visible and the diffusion coefficient was given by:

$$D_I = D_{S2}\left[1/P(q) - \chi/\chi_c\right] + \frac{kT}{6\pi\eta\xi}F(q\xi) \tag{2.9}$$

where χ_c is given by

$$1/\chi_c = 2x(1-x)\phi N \tag{2.10}$$

The first term in equation (2.9) represents the Rouse term as predicted by the simple Benmouna theory and is not new, the second term represents the long range hydrodynamic backflow effects which may be important in the critical region. $F(x)$ is the Kawasaki function which is nearly a linear function of x for $x \geq 2$, and approaches 0.75 as x approaches zero. This theory has not been extended to the general case of arbitrary

polymer molar mass, refractive index increment or composition, but one may reasonably assume that essential features of the theory will remain the same. In particular one can assume that there will be two contributions to D_I a Rouse term given by the simple Benmouna theory and an hydrodynamic term similar to the second term in equation (2.9). The Rouse term vanishes as the critical temperature is approached. The behaviour of the second term depends on the magnitude of $q\xi$;

(a) $q\xi << 1$, second term is q independent and does display a critical slowing down.

(b) $q\xi >> 1$, second term proportional to q and does display critical slowing down.

Miyashita et al [29] and Seils et al [42] have recently reported studies of ternary solutions close to phase separation. Miyashita et al used static light scattering and measured the critical exponent of the correlation length to be 0.63 which is very close to the three-dimensional Ising exponent (0.63) and obviously different from the mean-field or the Fisher's renormalised Ising exponents (0.50 and 0.71 respectively). Seils et al. investigated symmetric ternary solutions using both static and dynamic light scattering and found (from static light scattering measurements) the critical exponent of the correlation length to be 0.57 ± 0.02. These authors also found that close to phase separation the temperature dependence of χ could be expressed as

$$\chi = \chi^A / T + \chi^B \qquad (2.11)$$

where χ^A and χ^B are independent of temperature T.

2.1(c). The Mode Amplitudes

The mode amplitudes A_+, and A_- (see equation (2.1)), are complicated functions of the polymer molar masses, the polymer concentrations and the solution interaction parameters, moreover they also depend on the refractive indices of the polymers and the solvent. In the special case that polymer 1 is isorefractive with the solvent the amplitude of the fast mode, A_+, vanishes and the field auto correlation function of the scattered light reduces to a single exponential with decay rate governed by the interpenetration diffusion coefficient D_I. Furthermore if the visible polymer is present in trace amounts only then x approaches zero and D_I approaches D_{S2}, the self diffusion coefficient of the visible polymer.

Physical details of the polymers, the solvent and the solutions used in this work and in a previously published similar study by Nemoto et al. [30], are shown in Table 2.1. These two studies involve polymers of slightly differing molar masses, these differences must be taken into account when comparing the D_I values obtained from the two studies. Values for χ/υ and the second virial coefficient were not available for the solvent thiophenol so the corresponding values for toluene (taken from Konac et al. [27] and

Fukuda et al [21] respectively) were used instead. This is not expected to introduce significant error since the theoretical calculations are not very sensitive to these values provided the spinodal is not approached.

The fast wave amplitude, A_+ is non zero because polystyrene is not exactly isorefractive with the solvent. Figure 2.1 shows the predicted variation of the ratio of the fast and slow decay mode amplitudes, A_+/A_-, with total polymer concentration, c, for the semi-dilute solutions. The amplitude of the fast decay mode is always less than 4% of the slow decay mode amplitude so its presence is not expected to affect the observation of the slow mode. The fast mode will not be investigated here.

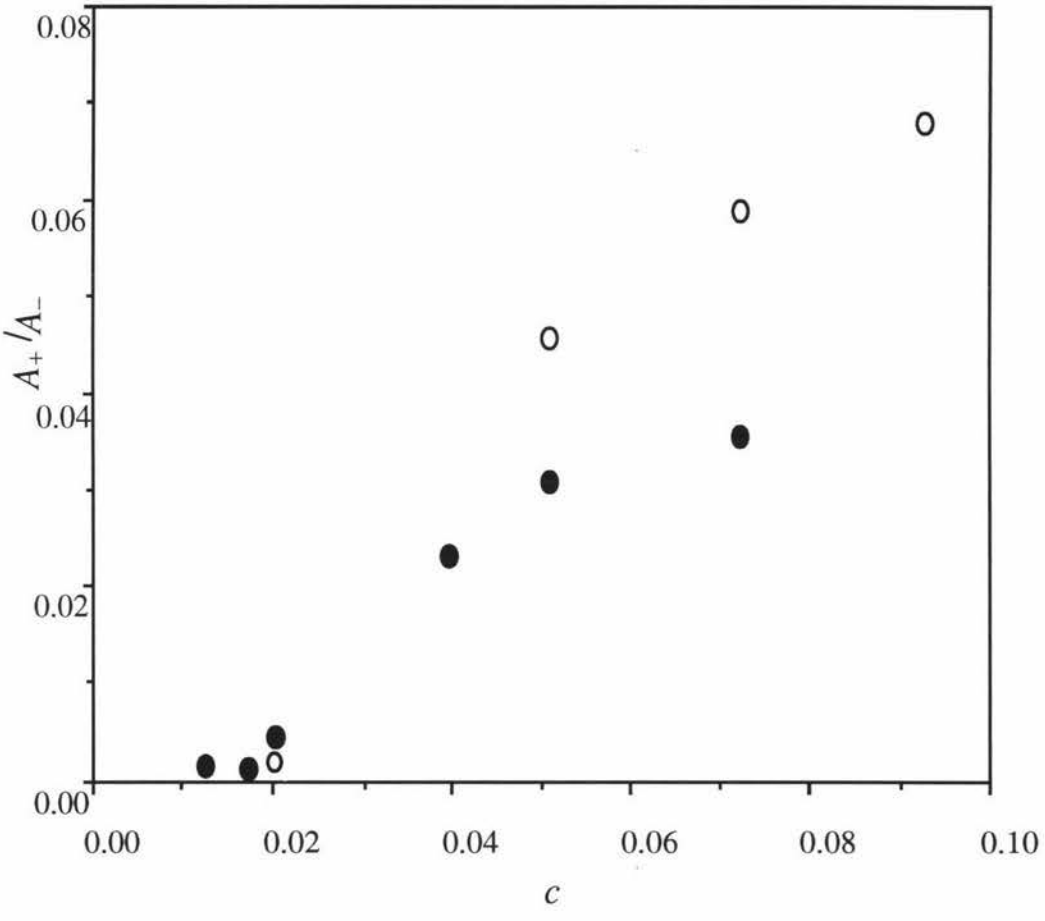

Figure 2.1 Variation of the ratio of the decay mode amplitudes, A_+/A_-, with total polymer concentration, c, for semi-dilute solutions studied here. Theoretical predictions from the Borsali-Benmouna theory. ● this work O Nemoto et al., see Table 2.1.

The theoretical variation of D_I/D_{S2} with total polymer concentration is shown in Figure 2.2 for the semi-dilute solutions, where D_{S2} is the self diffusion coefficient of the

PMMA. D_I is within 95% of D_{S2} for the semi-dilute solutions studied by Nemoto et al. [30], and within 98% of D_{S2} for the semidilute solutions studied here. The systematic differences in polymer molar masses used in the two investigations have compensating effects on the predicted values of D_{S2} and hence D_I. In the study by Nemoto et al. [30] the molar mass of the PMMA was 4% larger (so causing a 4% decrease in D_{S2}) and the molar mass of the polystyrene was 20% smaller (so causing a 5% increase in D_{S2}), Pinder [34]. Hence the self diffusion coefficient of the PMMA in the solutions studied by Nemoto et al. [30] are expected to be approximately 2% larger than that of the PMMA in the corresponding solutions studied here. This implies that the values of D_I found by Nemoto et al. [30] are expected to be only 2% larger than those observed here.

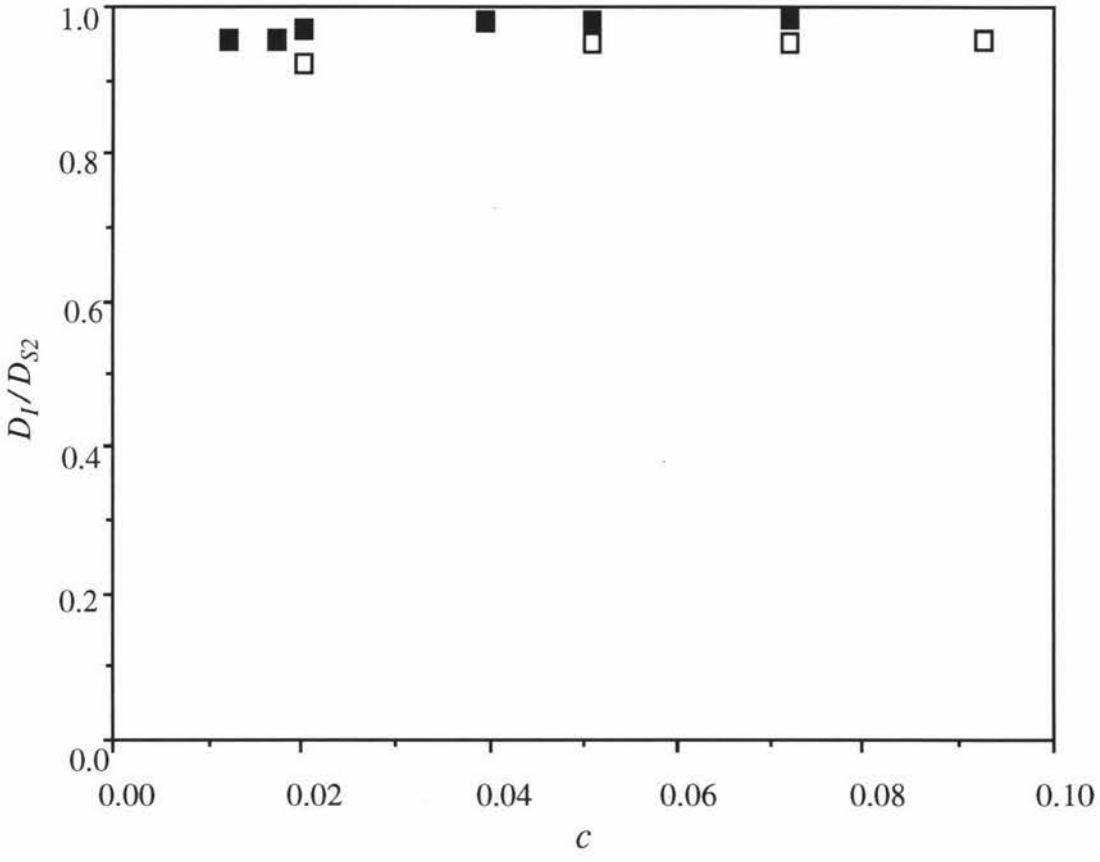

Figure 2.2 Variation of the normalised interpenetration diffusion coefficient, D_I/D_{S2}, with total polymer concentration, c, for semi-dilute solutions. Theoretical predictions from the Borsali-Benmouna theory. ■ this work, □ Nemoto et al., see Table 2.1.

Table 2.1 Details of ternary solutions formed with PMMA dissolved with polystyrene in thiophenol used in this work and in a previously published similar study by Nemoto et al..

Concentration Range (g/g^{-1})	**Polymers**	Molar Mass	Polydispersity	**$\partial n/\partial c$**
0.00442 - 0.0755	Majority Polymer Polystyrene	233 000	< 1.06	0.00742
(This Work)	Minority Polymer PMMA	330 000	1.1	-0.07895
0.00446 - 0.0992	Majority Polymer Polystyrene	185 000		0.00742
(Nemoto et al)	Minority Polymer PMMA	342 000	1.1	-0.07895

2.2 Ultra centrifugation

The theory describing ultra centrifugation of macromolecules in binary solutions is described by Fujita [20]. If the solute has a greater density than the solvent, then it migrates radially (outwards) when the solution is spun at extremely large angular speed in an ultra centrifuge. The solute molecules are said to "sediment" towards the "outerside" of the container due to the high centrifugal forces involved. In a single-component, non-interacting system this transport of molecules produces a region in the cell containing only solvent (supernatant) and a region in the cell where the concentration is uniform. This region of uniform concentration is called the plateau region. Between the supernatant and the plateau region is a transition zone, called the boundary, in which the concentration varies with distance from the axis of rotation. The migration of this boundary corresponds to the migration of the solute molecules. The boundary is usually observed using a Schlieren optical system and is often referred to as the "Schlieren peak".

Photographs of the Schlieren peak can be taken at appropriate time intervals using the Schlieren optical system. The sedimentation coefficient of the solute can be obtained by observing the migration of the Schlieren peak through the sedimentation cell and plotting

the natural logarithm of its distance from the axis of rotation against time, s is defined through

$$s = \frac{1}{\omega^2}\frac{d}{dt}\ln r \tag{2.12}$$

where ω, is the angular velocity in radians per second

t is the time in seconds, and

r is the distance of the boundary from the axis of rotation.

The Schlieren peak broadens as it migrates from the meniscus due to mutual diffusion of the solute and solvent hence the maximum height of the peak as well as the area under it decreases.

The theory of Fujita [20] assumes that the sedimentation coefficient of a single macromolecular species sedimenting in a low molar mass solvent decreases with polymer concentration as

$$s = s_0(1 - kc) \tag{2.13}$$

and predicts the following relationship for the mutual diffusion coefficient D:

$$G^{-1}(2r_0\omega^2 kc_0 s_0(H/A)t) = \frac{r_0\omega^2 kc_0 s_0}{2\sqrt{D}}[1 - \frac{s_0\omega^2 t}{2}(1 - kc_0)]\sqrt{t} \tag{2.14}$$

where r_0 is the initial position of the boundary, ω the angular speed of sedimentation, k the sedimentation friction coefficient, s_0 the infinite dilution value of the sedimentation coefficient and H/A the height to area ratio of the Schlieren peak.

The function $G(y)$ is given by:

$$G(y) = y[2y + \frac{2\exp(-y^2)}{\sqrt{\pi} + 2\int_0^y \exp(-y^2)dy}] \tag{2.15}$$

If the argument of $G(y)$ is sufficiently small, equation (2.14) can be approximated as

$$(A/H)^2 = 4\pi Dt(1 + s_0\omega^2 t) \tag{2.16}$$

thereby eliminating k. The diffusion coefficient D can be obtained from the initial slope of the graph of $(A/H)^2$ against $4\pi t$ if sufficient data can be collected at short sedimentation times. In practice this approximation is very delicate and its use may yield unreliable values of D, (see Fujita [20] for a detailed discussion of this point). It is preferable to use equation (2.14) without approximation if the variation of sedimentation coefficient with macromolecular concentration is known .

These relationships govern the sedimentation of a single macromolecular species dissolved in a low molar mass solvent. Following Nemoto et al [30] we assume they are also valid for ternary polymer solutions in which the majority polymer is both isorefractive and isopycnic with the solvent, and the visible polymer is present as a trace only. Thus the majority, invisible polymer does not sediment and this polymer and the solvent can be considered to constitute an "effective solvent" through which the minority, visible polymer sediments and diffuses. Under these circumstances s and c are interpreted as the sedimentation coefficient and concentration of the visible polymer respectively. The diffusion coefficient D is assumed to be D_I, the interpenetration diffusion coefficient of the polymers. D is obtained by observing the change in shape of the Schlieren peak with time. The area to height ratio of the Schlieren peak is used in equation (2.14) to obtain this diffusion coefficient of the polymers.

Two different methods were used to determine the area under each peak in this work. The first method was based on the assumption that each peak has a Gaussian profile, whilst the second made no assumption regarding the shape of the peak. Using the assumption that the peaks have Gaussian profiles, the area under each peak was found by integrating the standard Gaussian curve. All measurements needed for the integration were obtained using a Nikon comparator. Numerical integration was used to calculate the area under each peak in the second method. In each case the area under each peak was then divided by the appropriate instrument magnification factor. There were no significant differences between the areas found using the two methods and so the first method was routinely adopted in this study. The fact that the two methods yield the same value for the area indicates that the peak in the Schlieren pattern is indeed nearly Gaussian which in turn indicates that the dynamic processes in the solution were dominated by sedimentation and diffusion only. This confirms the assumption that the PMMA sediments and diffuses through an equivalent solvent of polystyrene and thiophenol. The area under each peak was then divided by the maximum peak height to yield the height to area ratio.

Since the sedimentation coefficient of the visible polymer through the "effective solvent" is very small (of the order of 10^{-14} s), sedimentation must be observed over long time scales at large angular speeds to facilitate the measurement of s. This means that the function $G(y)$ cannot be replaced by its argument and an estimate of k, the sedimentation friction coefficient is needed. This is not required to high accuracy since k appears on both sides of equation (2.14) and a measure of compensation occurs. If an inexact value is used then the graph of the left hand side of equation (2.14) against the right hand side is slightly non linear and $\sqrt{D}$ must be obtained from the initial slope.

Chapter 3
Preparation of Ternary Solutions

3.1 PMMA / PS /Thiophenol

This ternary solution system was previously studied by Nemoto et al.. They studied solutions formed with 342 000 molar mass PMMA dissolved with either 43 900 or 8420 000 polystyrene in thiophenol. This system was chosen because the majority polymer (polystyrene) and thiophenol were not only isorefractive but also isopycnic. They found k to be -0.07 and -0.04 respectively for those systems (refer to equation (2.13)).

The system chosen for this study was 330 000 molar mass PMMA and 233 000 molar mass polystyrene dissolved in thiophenol. This system was chosen because it approximated a system studied by Nemoto et al. The value of k for this system was estimated to be -0.06. Notice that these two studies involve PMMA samples of almost identical molar mass, but the polystyrenes, the majority polymer in each case, differ in molar mass by approximately 20%.

It is vital for all the glassware used in light scattering experiments to be clean in order to obtain accurate and reliable results. The procedure for cleaning the glassware used in this study is given below.

3.1.1 Cleaning of Glassware

It is well known that particulate contamination of light scattering samples can severely distort the collected data due the fact that not only the particles being studied but also any other particles present in the scattering volume contribute to the scattered light. Therefore it is necessary to ensure that both the sample itself and its container are free of such contamination before experiments are performed. The procedures used for cleaning the light scattering cells in this work are described below.

The NMR tubes (5 mm), conical flasks (5 ml), glass syringe, stainless steel needles and the stainless steel filter holder (Millipore Swinny) were first washed with detergent and water and then soaked in chromic acid and left overnight to remove any residue still remaining in the glassware. They were then removed from the chromic acid and washed thoroughly in water before rinsing with distilled water and then with analytical grade acetone. They were then flushed with condensing acetone vapour using the apparatus

shown in Figure 3.1. This was done to remove all dust particles from the glassware. Each item of glassware, still inverted, was then transferred to a desiccator to be dried and stored. Flushing with condensing acetone vapour was performed in a cleaned fumehood presuming that it provided a dust free environment.

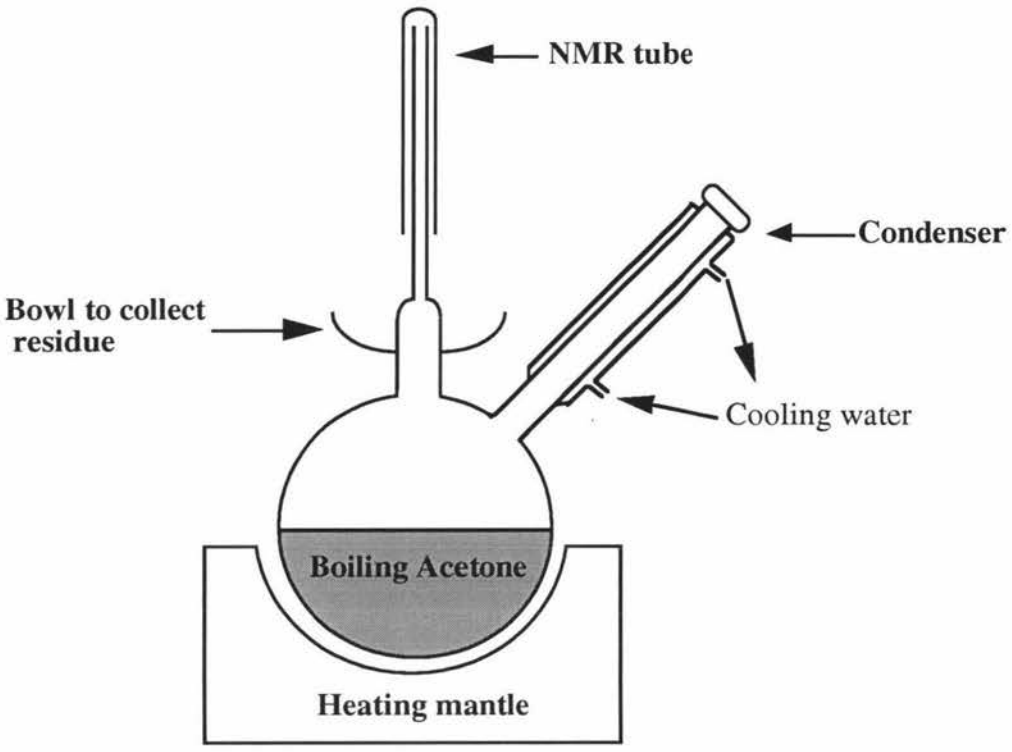

Figure 3.1 Apparatus for cleaning glassware.

3.1.2 Preparation of the samples.

The PMMA and polystyrene were weighed in a clean conical flask (5 ml) using a Mettler AT261 balance because of very small masses of polymers (of the order 10^{-3}g) needed to make up the required concentration. The polymers were then dissolved in 2 millilitres of thiophenol and the whole mixture was then weighed to obtain the mass of thiophenol used. The solution was left over night to allow the polymers to be completely dissolved. Dilute and semi-dilute solutions were formed in which the polystyrene was the majority polymer and the PMMA concentration was constant at approximately 0.001 gram per gram of solvent. Preparations of the solutions were carried out in a fumehood because of the toxicity of thiophenol and its strong and unpleasant odour. All concentrations are specified in grams of polymer per gram of solvent.

About 1 ml of the solution was then transferred to the cell to be used in the ultracentrifuge using cleansed glass syringe and stainless steel needle. In practice, the

filled cell was always left overnight before any measurements were taken. About 0.5 ml of the solution was needed for the light scattering studies. The solutions were filtered directly into the scrupulously cleansed NMR tubes using a 0.2 μm millipore filter held in the stainless steel filter holder (Millipore Swinny). Cleansed glass syringe and stainless steel needles were also used to filter the samples. The first few drops of the sample were discarded before filling the tube. The tube was filled to a depth of just above the curved bottom. The minimum possible amount of sample was used to ensure that convection currents within the sample were kept to a minimum. The tubes were then flame sealed and stored at 25°C until light scattering measurements were taken.

3.2 PVME / PS / Thiophenol

Poly(vinyl methyl ether) (PVME) has been the subject of many experimental studies because of its compatibility with polystyrene both in blends and in ternary solutions with appropriate solvents. PVME is available only as a polydisperse and relatively poorly characterised raw material. The polydispersity of the original material can be reduced by fractional precipitation.

3.2.1 Fractionation

The fractionation of a polydisperse sample of polymer into fractions with narrower molecular weight distributions can be achieved in many different ways. A general discussion of fractionation techniques is provided by Flory [19].

The solvent quality of a polymer solution can be changed by varying either the composition of the solvent or by varying the temperature. The method of fractional precipitation exploits the variation of the precipitation temperature (or solvent composition) with molar mass. The method of fractional precipitation adopted in this work followed very closely the method used by Daivis [16] which relies on a change in solvent quality at constant temperature. The polymer is dissolved and a non-solvent is then added to the solution until the solvent quality has been reduced to the extent that precipitation occurs. At this point, the higher molar mass material precipitates and the lower molar mass molecules remain in solution. The solution is allowed to achieve equilibrium and slowly separates into two phases, one containing the dissolved lower molar mass fraction (supernatant) and the other containing the precipitated higher molar mass fraction. The precipitated phase actually contains much more solvent than polymer; the concentration of polymer in it may be only about 10 percent. The two phases can then be separated by removing the supernatant or the precipitate.

In this work, the polydispersity of PVME was reduced by removing the low and high molar mass portions of the distribution using fractionation techniques. The following equipment was used in the fractional precipitation; 1 litre 3-necked round bottomed flask, a precise temperature controller (Thermomix 1460, B.Braun, Melsungen AG West Germany), an overhead stirrer, and a glass water bath. The set-up of the equipment is shown in Figure 3.2.

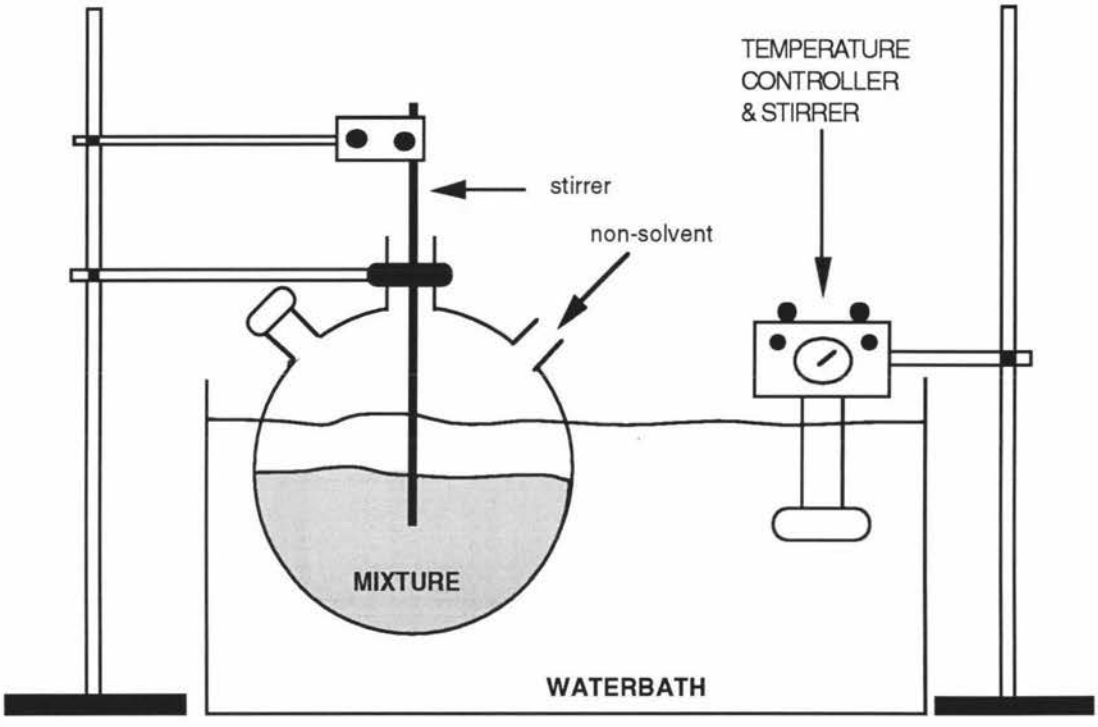

Figure 3.2 Apparatus for fractionation.

The procedure used in the fractional precipitation was as follows. About 10 grams of the raw material was dissolved in 100 ml of analytical grade toluene in the 1 litre 3-necked flask. The flask was then placed in the water bath maintained at 25°C. The solution was stirred vigorously as the non-solvent (petroleum spirit, analytical grade) was gradually added. Precipitation was first observed after the addition of approximately 450 - 500 ml of petroleum spirit. The mixture was adjusted by additions of small quantities of petroleum spirit and then warmed by a few degrees until the precipitate dissolved. The solution was then returned to the original temperature (25°C) and the precipitate which reformed was allowed to settle and then separate. This ensures that the precipitated fraction is not broadened by local precipitation during addition of the non-solvent. After the precipitated phase had settled, the supernatant was removed from the flask with a large glass syringe and stored in a clean container, taking great care not to disturb the

precipitate. The precipitate was then redissolved in toluene and completely removed from the flask and discarded. The flask was rinsed with toluene and then with the non-solvent before returning the supernatant into it for the next precipitation.

As before, more non-solvent (approximately 150 ml) was added to the supernatant to produce the next fraction. When the precipitate phase had settled, the supernatant which contained the low molar mass portions was removed from the flask and discarded. The precipitate (the middle fraction) was retrieved and then redissolved in 100 ml of toluene. This solution was then transferred to a smaller flask for drying.

3.2.2 Drying of the PVME

The sample of PVME was dried using a rotary evaporator. The flask containing the dissolved PVME was attached to the rotary evaporator using an "adaptor" and with the vacuum pump running. The flask was then lowered into a waterbath which was slowly heated to 30°C. Great care was taken so that the solution did not boil vigorously and spill into the evaporator. The solution boiled after 10 - 15 minutes, the temperature was then increased to 90 - 95°C, the speed of rotation was increased and the flask was evaporated for two hours. This allowed the solvent to evaporate and the polymer to spread in a thin layer around the wall of the flask.

After two hours, the sample was removed from the rotary evaporator and dried under a pressure of 0.2 mm Hg for a few hours to remove residual solvent. The flask was wrapped with aluminium foil during this process to prevent exposure to sunlight because PVME is susceptible to oxidative degradation. The aluminium foil was removed and the mass of PVME was measured and then the polymer was dissolved in 30 ml of thiophenol. The flask was rewrapped in aluminium foil and this stock solution was stored in cool, dark place.

3.2.3 Preparation of the samples

1.462 gram of PVME were obtained from fractionation and the mass of 30 ml thiophenol was 32.565 g. Therefore the concentration of the stock solution was 0.0430 gram of PVME per gram of solution.

The PVME and polystyrene were weighed in a clean 5 ml conical flask using the same balance that was used for the PMMA / PS system. The mass of PVME was obtained from the concentration of the stock solution. The polymers were then dissolved in 2 millilitres of thiophenol and the whole mixture was then weighed to obtain the mass of thiophenol used. The solution was left over night to allow the mixture to equilibriate. Dilute and semi-dilute solutions were formed in which the concentration of polystyrene (majority

polymer) was varied and the PVME concentration was constant at approximately 0.002 gram per gram of solution. The concentrations of some of the solutions were increased by leaving an open cell containing the solution under vacuum for a period of time. Some of the solvent was lost through evaporation but the polymer content was unchanged.

Again, preparations of the solutions were carried out in a fumehood because of the toxicity of thiophenol and its strong and unpleasant odour. All concentrations are specified in grams of polymer per gram of solution.

The procedures carried out in filling the cells for the ultracentrifuge and the light scattering studies for the PMMA / PS system were again adopted for this system too. The molar mass of this PVME fraction was 110 000 g/mol and the molar mass of polystyrene was 233 000 g/mol.

The polystyrene and PMMA used in this study were purchased from The Pressure Chemical Company and Polymer Laboratories respectively. Details of the molar masses and polydispersities are given in Table 2.1. The refractive index increments of the polymers are also given in Table 2.1. The solvent, thiophenol UN-No 2337, was purchased from Riedel-de-Haen. The photographic glass plates were purchased from the Eastman Kodak Company, Rochester USA. The PVME was donated by from GAF Pty Ltd, Grey Lynn, Auckland, New Zealand. The commercial product name of this sample was M-555.

Chapter 4
Dynamic Light Scattering Studies

4.1 Introduction

Dynamic light scattering (DLS) is a non-perturbing process based on the high-speed processing of stochastic optical signals scattered from a sample of the solution under study. It is performed on only very small quantities of sample which is required to be suspended in a clear liquid to enhance scattering.

In a typical DLS experiment, a sample of the solution to be studied is placed in a temperature controlled bath in the direct path of a laser beam. When the laser impinges on the sample, the electric field of the laser light induces an oscillating polarisation of the solute molecules which subsequently reradiate (scatter) light. The scattered light then enters a detector aligned at angle θ with respect to the transmitted beam as shown in Figure 4.1. The incident laser beam and scattered light are polarised with the electric field of the light perpendicular to the plane of the diagram.

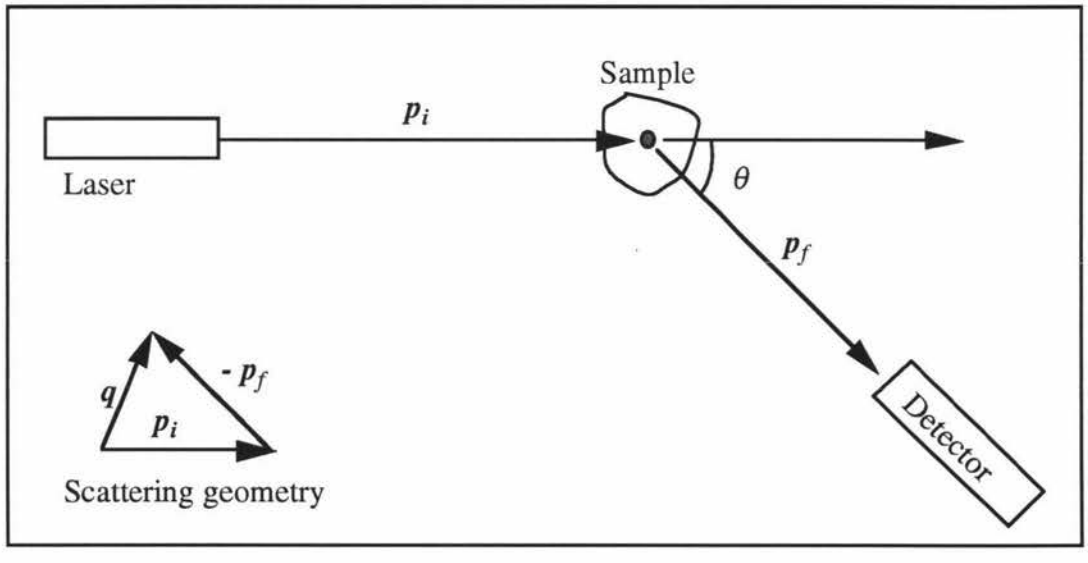

Figure 4.1 A schematic representation of the scattering system and geometry.

The reradiated (or scattered) light field at the detector at a given time is the sum (superposition) of the electric fields radiated from all the solute molecules in the scattering

volume and consequently depends on the exact positions of the molecules. The molecules are perpetually translating, rotating, and vibrating by virtue of thermal interactions. Because of this motion the positions of the radiators are constantly changing so that the total scattered electric field at the detector fluctuates in time. The scattered light is converted by the detector into data appropriate for processing by means of photon counting. These data are then processed by a signal analysis system and displayed as a correlation function which provides a concise method for expressing the degree to which dynamic properties are correlated over time. This property makes the correlation function the most important mathematic tool available in dynamic light scattering experiments.

The frequency shifts, the angular distribution, the polarisation, and the intensity of the scattered light are determined by the size, shape, and molecular interactions in the scattering material. Dust can be a major source of error in light scattering since dust particles are large compared to the particles to be studied, so dust contributes a scattered intensity which is much greater than that from the scatterers of interest. This would lead to misdiagonis of data. Obviously, cleaned samples are needed to alleviate this problem.

DLS is a useful means for investigating the dynamical behaviour of polymers in ternary solutions. This technique can be used to find both the cooperative and the interpenetration diffusion coefficients of polymers in a suitable ternary polymer solution. However, if the majority polymer is isorefractive with the solvent and the visible polymer is present in very small quantities only, then the amplitude of the fast decay mode is too small for it to to be observed so the cooperative diffusion coefficient cannot be found and only the interpenetration diffusion coefficient is susceptible to measurement. In this case the magnitude of the interpenetration diffusion coefficient approaches the self diffusion coefficient of the visible polymer.

A detail discussion of DLS theory can be found in a book by Berne and Pecora [6] and several collections of lectures and conference proceedings in this field (Pecora [32]), (Cummins and Pike [15]), (Pusey and Vaughan [37]), and (Deigorgion, Corti and Giglio [18]). This chapter presents an analysis of the system and reviews the intensity statistics obtained in typical dynamic light scattering experiments. A brief introduction of the signal analysis system is also given.

4.2 Dynamic Laser Light Scattering

The incident laser beam has an electric field vector of the form

$$\boldsymbol{E}(x,t) = \boldsymbol{e}_y E_0(x,y) e^{(ipz - i\omega t)} \tag{4.1}$$

where $\boldsymbol{e}_y$ is the unit vector in the direction of the polarisation (or electric field) vector; p denotes the magnitude of the propagation vector equal to $\frac{2\pi}{\lambda}$, λ and ω are the wavelength and angular frequency of the incident laser light, and t is the time.

The scattered light can be observed by a point detector placed in the (z, x) plane at a scattering angle θ with respect to $\boldsymbol{e}_z$, where $\boldsymbol{e}_z$ is the unit vector in the direction of beam propagation. For quasi-elastic light scattering, the magnitude of the final wave vector or the final propagation constant is equal to the magnitude of the incident wave vector and is given by p.

This scattering process involves an initial wave vector in the direction of propagation of the incident wave

$$\boldsymbol{p}_i = p\boldsymbol{e}_z \tag{4.2}$$

and a final wave vector in the direction of propagation of the wave that reaches the detector

$$\boldsymbol{p}_f = p\boldsymbol{e}_x \sin\theta + p\boldsymbol{e}_z \cos\theta \tag{4.3}$$

The vector $\boldsymbol{q}$ is defined in terms of the scattering geometry shown in Figure 4.1 as

$$\boldsymbol{q} = \boldsymbol{p}_i - \boldsymbol{p}_f \tag{4.4}$$

It is assumed that the photon energy is unchanged in the scattering process so that

$$|\boldsymbol{p}_i| = |\boldsymbol{p}_f|$$

Thus the magnitude of $\boldsymbol{q}$ can be found from the law of cosines,

$$q = |\boldsymbol{q}| = |\boldsymbol{p}_i - \boldsymbol{p}_f| = 2p\sin\left(\frac{\theta}{2}\right) \tag{4.5}$$

which may be varied between zero and $4\pi/\lambda$ by a proper choice of θ, the scattering angle.

The light scattered by the single particle j can be characterised by a scattering amplitude b_j and an optical phase determined by the scalar product of particle position x_j and scattering vector $\boldsymbol{q}$:

$$\boldsymbol{E}_j(\boldsymbol{q},t) = \boldsymbol{e}_y E_0(x_j,y_j) b_j e^{(i\boldsymbol{q}\cdot\boldsymbol{x}_j - i\omega t)} \tag{4.6}$$

Assuming that the scattering process does not change the initial state of polarisation (or using a suitable polariser in front of the detector), and omitting the vector character of the field as well as its explicit time dependence, the scattered light can be expressed as:

$$u_j(\boldsymbol{q},t) = E_0(x_j,y_j) b_j e^{i\boldsymbol{q}\cdot\boldsymbol{x}_j} \tag{4.7}$$

The weak focusing of the illuminating beam makes $E_0(x_j, y_j)$ a weakly varying function of particle position. The temporal behaviour of the complex amplitude is clearly dominated by changes of the phase factor, and it is quite useful to absorb $E_0(x_j, y_j)$ into a new scattering amplitude

$$a_j = E_0(x_j,y_j) b_j \tag{4.8}$$

This scattering amplitude a_j now contains the whole geometry of the experiment, including the particle position x_j within the beam, as well as the beam power and the form factor, which describes the scattering of the particle j for a scattering vector $\boldsymbol{q}$.

To make a connection between molecular properties and light scattering measurements it is convenient to introduce the assumption that the light is scattered from particles and that the dielectric constant fluctuations are due solely to fluctuations in the number density of particles. For the N particle system, we need to sum the scattered amplitudes of all N particles in the measurement volume to obtain a complex amplitude

$$u_f(\boldsymbol{q},t) = \sum_{j=1}^{N} a_j\left(x_j\right) e^{i\boldsymbol{q}x_j} \tag{4.9}$$

Note the implicit time-dependence of this amplitude due to motion of the particles, that is, the $\boldsymbol{x}_j$ are functions of time $\boldsymbol{x}_j(t)$. After few assumptions (Berne and Pecora [6]) and the use of the complex temporal autocorrelation mathematics, we can determine the statistical properties of the complex amplitude $u_f(\boldsymbol{q},t)$ as a function of time.

The complex amplitude $u_f(\boldsymbol{q},t)$ not only yields Gaussian statistics if considered at a single time, but also the two-time probability density yields joint Gaussian statistics. More importantly, the procedure just outlined can be continued to prove all higher-order statistics to be Gaussian. This scattering process thus engenders scattered light whose statistics are Gaussian.

This property, the common occurrence of Gaussian statistics for the complex amplitude at the detector in light scattering experiments, underlines the great practical importance of autocorrelation measurements. The temporal electric field autocorrelation function

$$G^{(1)}(t) = \langle u_f(0) u_f(t)^* \rangle \tag{4.10}$$

is the lowest-order time-dependent moment. All higher-order moments may be decomposed into expressions involving just the temporal autocorrelation function $G^{(1)}(t)$, also known as amplitude or first-order correlation function.

Because of these results, we can focus our discussion on the intensity or second-order correlation, which is amenable to measurement.

$$G^{(2)}(t) = \langle |u_f(0)|^2 |u_f(t)|^2 \rangle \tag{4.11}$$

Such a moment is obtained by summing over all possible distinct permutations of the amplitudes involved. Non-zero expectations are only obtained for pairs of amplitudes, where the members of the pair are complex conjugate. The following very important result is obtained:

$$\begin{aligned} G^{(2)}(t) &= \langle |u_f(0)|^2 \rangle \langle |u_f(t)|^2 \rangle + \langle u_f(0) u_f(t)^* \rangle \langle u_f(0)^* u_f(t) \rangle \\ &= G^{(1)}(0)^2 + |G^{(1)}(t)|^2 \end{aligned} \tag{4.12}$$

which is the well known Siegert relation [25]. It gives the relationship between the amplitude correlation, which is related to the physical attributes of the solution, and the intensity correlation function which can be measured in a photon correlation experiment. Hence the time dependence of the dielectric constant fluctuations can be studied by measuring the intensity autocorrelation function.

4.2.1 Intensity and amplitude autocorrelation function

The temporal first-order autocorrelation function for the case of non-interacting scattering particles undergoing individual Brownian motion can be easily calculated. This is an adequate model for all suspensions at sufficient dilution. Brownian motion of a colloidal particle is driven by molecular collisions. The random character of this driving force results in a highly irregular particle motion. The velocity autocorrelation function of a Brownian particle decays on a time-scale of the order

$$t_r = \frac{m}{6\pi\eta a} = \frac{\rho a^2}{9\eta} \tag{4.13}$$

known as the hydrodynamic relaxation time (Pecora [32]). Here m denotes the mass, a the radius, ρ the density of the particle, and η is the viscosity of the solvent.

Usually t_r is much less than typical time scales accessed in photon correlation experiments. Hence we may expect particle displacements on our time-scale to be composed of very many independent small displacements. Application of the central limit theorem then predicts Gaussian statistics for each particle displacement δx_j with a second moment that increases linearly with time:

$$\left\langle \delta x_j^2 \right\rangle = 6Dt \tag{4.14}$$

The proportionality factor is six times the particle diffusion coefficient:

$$D = \frac{k_B T}{6\pi\eta a} \tag{4.15}$$

where $k_B T$ is the average energy in a single degree of freedom of a physical system at equilibrium and k_B is the Boltzmann constant. Treating the far-field complex amplitude as a sum over N single-particle contributions, the first-order or amplitude correlation function becomes

$$G^{(1)}(t) = N\left\langle \left|a_j\right|^2 \right\rangle e^{-q^2 Dt} \tag{4.16}$$

where we have used the different time-scales of the a_j and the phase factors to separate their expectations, and the statistical independence of x_j and x_m for j not equal to m to eliminate non-diagonal terms in the double sum. The final expectation over the phase factor is then recognised as the spatial Fourier transform of the particle displacement $\delta x_j(t)$ over a time interval t, which yields an autocorrelation function that is a Gaussian in q and a negative exponential in t. The corresponding normalised first-order correlation function reads (Berne and Pecora, 1976)

$$g^{(1)}(t) = e^{-q^2 Dt} \tag{4.17}$$

Using the Siegert relation, the second-order correlation of the spatially integrated intensity can be obtained

$$G^{(2)}(t) = \langle I \rangle^2 \left[1 + \beta e^{-2q^2 Dt}\right] \tag{4.18}$$

where β is called the intensity intercept. It is nonunity due to instrumentation effects such as incomplete coherence. Equation (4.18) can be rewritten as

$$G^{(2)}(t) = B\left[1 + \beta e^{-2q^2 Dt}\right] \tag{4.19}$$

where B is the baseline, a second instrumentation effect. In normalised form

$$g^{(2)}(t) = \beta e^{-2q^2 Dt} \tag{4.20}$$

The intensity correlation function can be estimated by performing a photon correlation experiment. The analysis in terms of a negative exponential readily yields the diffusion coefficient and hence the size of the colloidal particles.

4.2.2 Data analysis of single decay rate system

Eqn (4.17) can be rewritten in a more general form to generally treat the data in terms of decay rates Γ

$$g^{(1)}(t) = e^{-\Gamma t} \tag{4.21}$$

then eqn (4.19) becomes

$$G^{(2)}(t) = B(1 + \beta e^{-2\Gamma t}) \tag{4.22}$$

This relationship is fitted to the data to provide an estimate of the parameter of interest Γ. Basically this can be done in two different ways, either a linear or a non-linear method, depending on whether the value of the baseline is reliably known or not.

If B is reliable and known with sufficient precision, then the simplest way to determine Γ is to transform the data into

$$\ln\left(\frac{G_2(t)}{B} - 1\right) = \ln\beta - 2\Gamma t \tag{4.23}$$

and to fit eqn (4.23) as a linear function of t, with -2Γ the slope and lnβ the intercept.

This linear method has the disadvantage that for values of $G^{(2)}(t)$ close to B (ie. for large t), $G^{(2)}(t)/B - 1$ is very small, which greatly enhances the scatter of the data and introduces some uncertainty in the values of the fitted parameters. Moreover, this procedure is very sensitive to the correct value of B.

Better results can be obtained with a non-linear method, where an initial guess for the parameter Γ is introduced and its value corrected in successive iterations until the desired precision is reached. In this procedure all the three parameters Γ, β, and B are determined by the fit, and no assumption is made about the baseline (Rektorys, 1976), (Press, 1986).

Once the results of the fit are obtained, the goodness of fit has to be analysed. Most descriptive for this purpose is a distribution of residuals,

$$\varepsilon = G^{(2)}(t) - f(t) \tag{4.24}$$

where $f(t) = B\left(1 + \beta\left|g^{(1)}(t)\right|^2\right)$ are the calculated values of the correlation function.

4.3 Relationship between the photon correlation function and the intensity correlation function

4.3.1 Conversion of scattered light into appropriate processing data

As mentioned in the last section, the intensity correlation function can be obtained from the light scattering experiment, and can be used to calculate the diffusion coefficient of the scattering material. Normally the intensity correlation function can not be obtained directly from experiment, rather the photon correlation function is determined.

The scattered light from the particles of the scattering material causes ejection of photo-electrons in the detector system (photomultiplier tube) and subsequently produces voltage pulses. These voltage pulses are then processed by a preamplifier and discriminator to produce single a TTL level pulse of 25ns duration for each detected photon (see Figure 4.2). The preamplifier and discriminator are both incorporated in the photomultiplier tube.

The resulting output of the photomultiplier tube consists of a random train of pulses corresponding to the photons detected. Samples of duration ΔT are obtained by integrating all the incoming pulses over the time interval ΔT, using specially designed counters. The sample time ΔT is set by a sample time clock (STC). The data recorded in the counter are transferred to the subsequent processing instrument (correlator).

At the end of each sample time, the counter is reset for the next sample. In this method the incident data are all treated identically, and the samples are non-overlapping and hence independent. Poisson statistics are obeyed for the number of photon detection pulses. This process can be cycled repetitively until enough samples have been taken to give an adequate estimate of the desired information. The counter system model shown in Figure 4.2 was used to process the data.

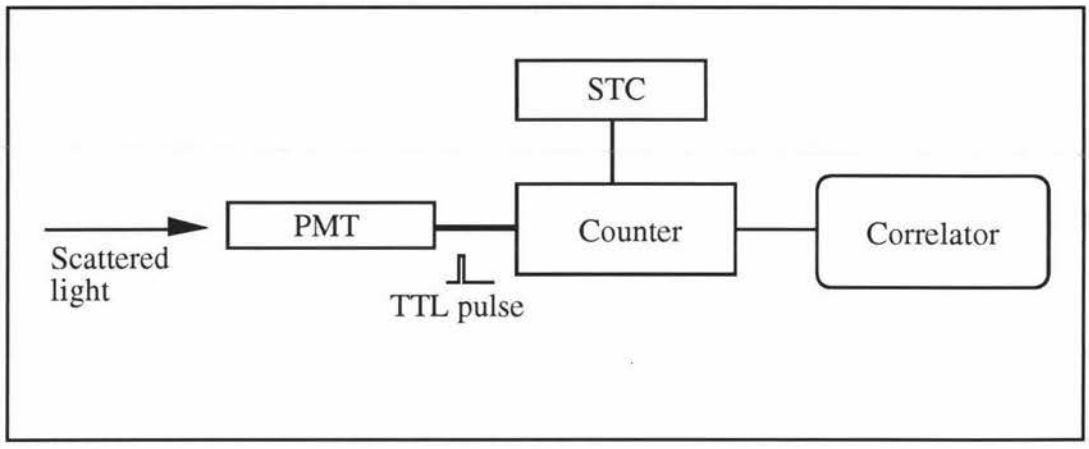

Figure 4.2 The counter system

Figure 4.3 shows the output pulses of the photomultiplier tube and the corresponding response of the counter with respect to the sample time ΔT

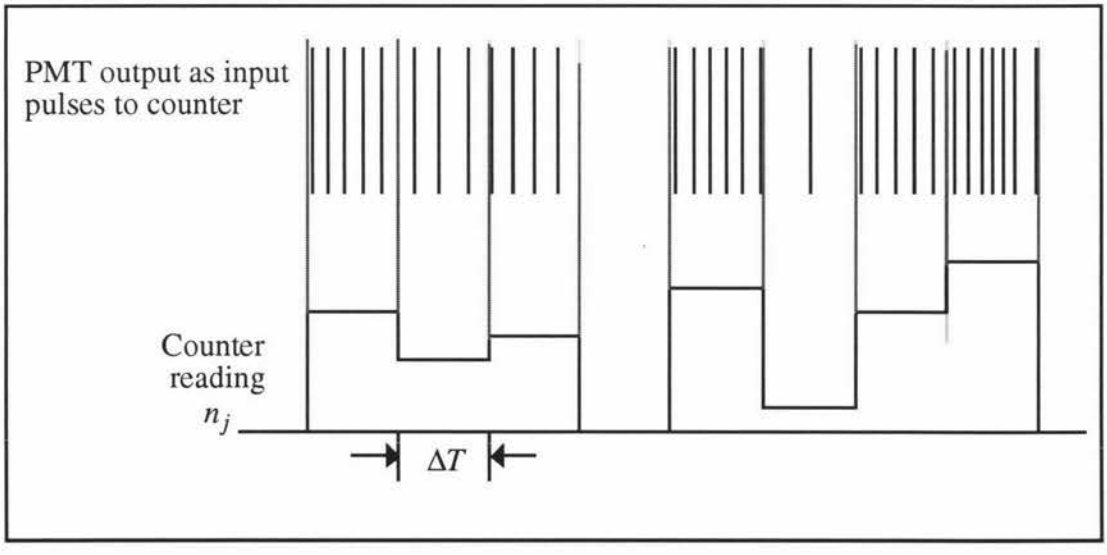

Figure 4.3 Photon counting

4.3.2 Equivalence of photon correlation and intensity correlation

Assume n_j is the number of photon detection pulses counted during a particular sampling time interval $j\Delta T$, and that such an ordered sequence of random variables n_j is a realisation of a stochastic process. Then

$$G_n(k) = \langle n_j n_{j+k} \rangle = \langle n_j n_{j-k} \rangle \tag{4.25}$$

is known as the autocorrelation function of the stochastic process, or the photon correlation function.

Each photon detection event is essentially independent of all the others so pulse arrival times are expected to be completely random. Hence the number of photon detection pulses counted during some finite sample time interval ΔT is expected to be governed by Poisson statistics. If I denotes intensity (expressed as the average number of photons reaching the detector in unit time) and p is the quantum efficiency of the detector, then the mean number of detected pulses per sample time ΔT is simply

$$\langle n \rangle = \mu = pI\Delta T \tag{4.26}$$

The mean is given by the time integral of the intensity over the sample time interval:

$$\langle n_j \rangle = \mu_j = p\int_{(j-1)\Delta T}^{j\Delta T} I(t)dt \tag{4.27}$$

Hence using basic statistical theory, and assuming stationarity for $I(t)$ (Berne and Pecora, 1976):

$$\langle n_j n_{j-k} \rangle_n = \delta_{k0} \langle \mu_j \rangle_\mu + \langle \mu_j \mu_{j-k} \rangle_\mu \tag{4.28}$$

where $\langle ... \rangle_\mu$ denotes averages over intensity statistics and $\langle ... \rangle_n$ is averages over photon statistics. $\delta_{k0} \langle \mu_j \rangle_\mu$ vanishes for non-zero k. Eqn (4.28) is an expression of the equivalence of photon correlation and intensity correlation. This connection between time-averaged intensities and photon counting statistics is a most important rule of light scattering.

This equality is the very basis of the photon correlation technique. It makes it possible to analysis the intensity correlation function by means of the measured photon count correlation function.

4.3.3 Linear photon correlation function

In a DLS experiment, the photon correlation function $G_n(k)$ is not obtained directly. Instead a finite number of samples M of the photon count are obtained over some finite total measurement time $T_m = M\Delta T$. The most common algorithm used to calculate the real-time correlation function yields a photon correlation estimator

$$G_e(k) = \frac{1}{M}\sum_{j=1}^{M} n_j n_{j-k} \tag{4.29}$$

at a lag time $k\Delta T$. The subscript 'e' is used to denote estimators. $G_e(k)$ constitutes an unbiased estimator for the photon correlation function $G_n(k)$. The expectation of $G_e(k)$ is

$$\langle G_e(k)\rangle = G_n(k) = \langle n_j n_{j-k}\rangle \tag{4.30}$$

No measurement will yield estimator data $G_e(k)$ exactly equal to $G_n(k)$, there will always be some statistical error $G_e(k) - G_n(k)$ (Schatzel [48]). At small lag times, M has almost always to be a very large number (10^6 or more) in order to obtain sufficient averaging over photon counting noise.

4.4 Correlator

As mentioned earlier, the data recorded by the counter are transferred to the correlator to be processed. The correlator hardware performs four basic tasks: (1) count input pulses over sampling intervals spaced on some grid defined by a sample time ΔT; (2) delay these counts for some lag time $k\Delta T$; (3) multiply current input counts with the delayed counts; (4) accumulate these products; that is, calculate their sum. One accumulation must be performed during each sample time for each channel for real time implementation of the autocorrelation function. A model of a linear correlator is shown in Figure 4.4.

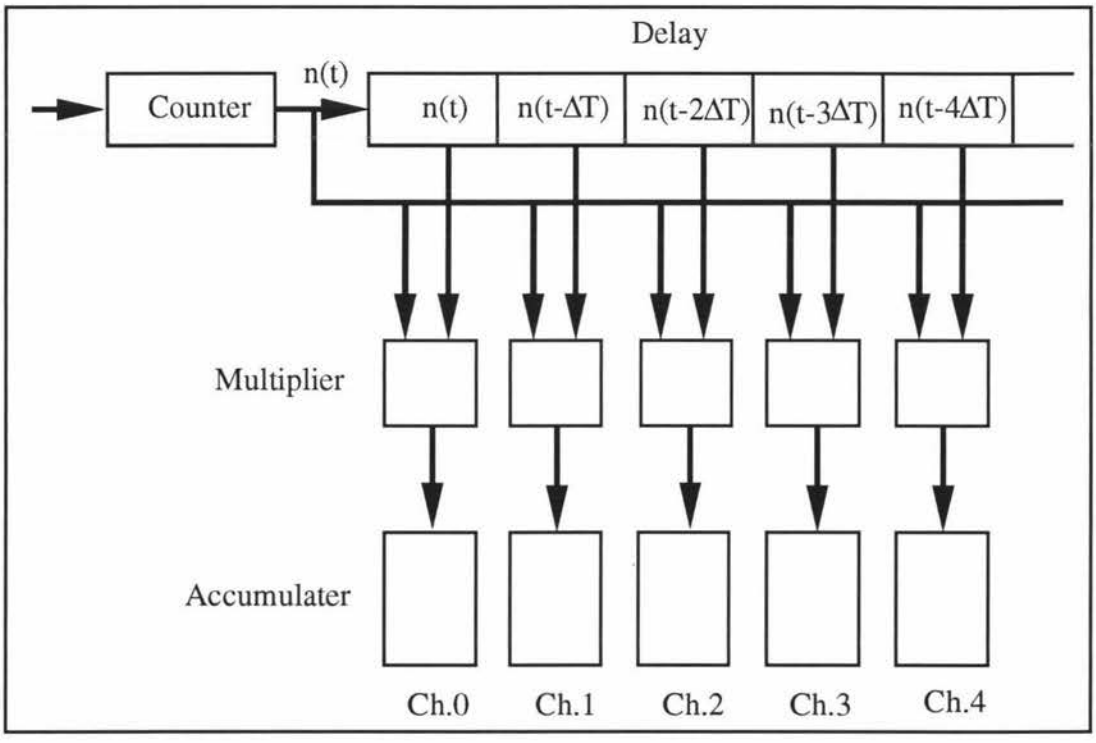

Channel 0: $G(0) = \sum n(t)\, n(t)$

Channel 1: $G(1\Delta T) = \sum n(t)\, n(t-\Delta T)$

Channel 2: $G(2\Delta T) = \sum n(t)\, n(t-2\Delta T)$

Channel 3: $G(3\Delta T) = \sum n(t)\, n(t-3\Delta T)$

Channel 4: $G(4\Delta T) = \sum n(t)\, n(t-4\Delta T)$

Figure 4.4 Linear correlator model

Obviously the lag time range of a linear correlator is limited by the number of correlation channels used. This is not a problem for applications where the correlation function consists of a single exponential. However processes exist which have important spectral information in a lag time range of $1{:}10^{10}$. To obtain reliable time discrete correlation functions for such processes, a linear correlator would need to have at least 10^{10} channels to maintain resolution. Cost and size limitations would make such a device unrealisable with present day electronics.

4.4.1 Clipping correlator

The correlator used in this study was a clipping correlator build by R.C. O'Driscoll in 1970's in the Department of Physics, Massey University. This technique was developed

in the 1970's and the correlator is still successfully used in DLS experiments. This kind of correlator can work at very short sample times, 50ns, in real time.

There are two techniques used in this kind of correlator. The first involves the clipping of the delayed signal to single-bit accuracy before the correlation function is computed (Oliver [14]). The output of a clipper is '0' if the number of counts detected in a given sample time ΔT is less than or equal to the clipping level, and '1' if the number of counts detected exceeds the clipping level.

The second technique takes advantage of clipping to simplify multiplication. If n_c is the direct signal (the number of count pulses into the system), and n' is the clipped delayed signal ('1' or '0'), then the required multiplications can be replaced by a series of additions:

$$n_c n' = \sum_{n'} n_c \tag{4.31}$$

These additions are triggered by the input pulses n'.

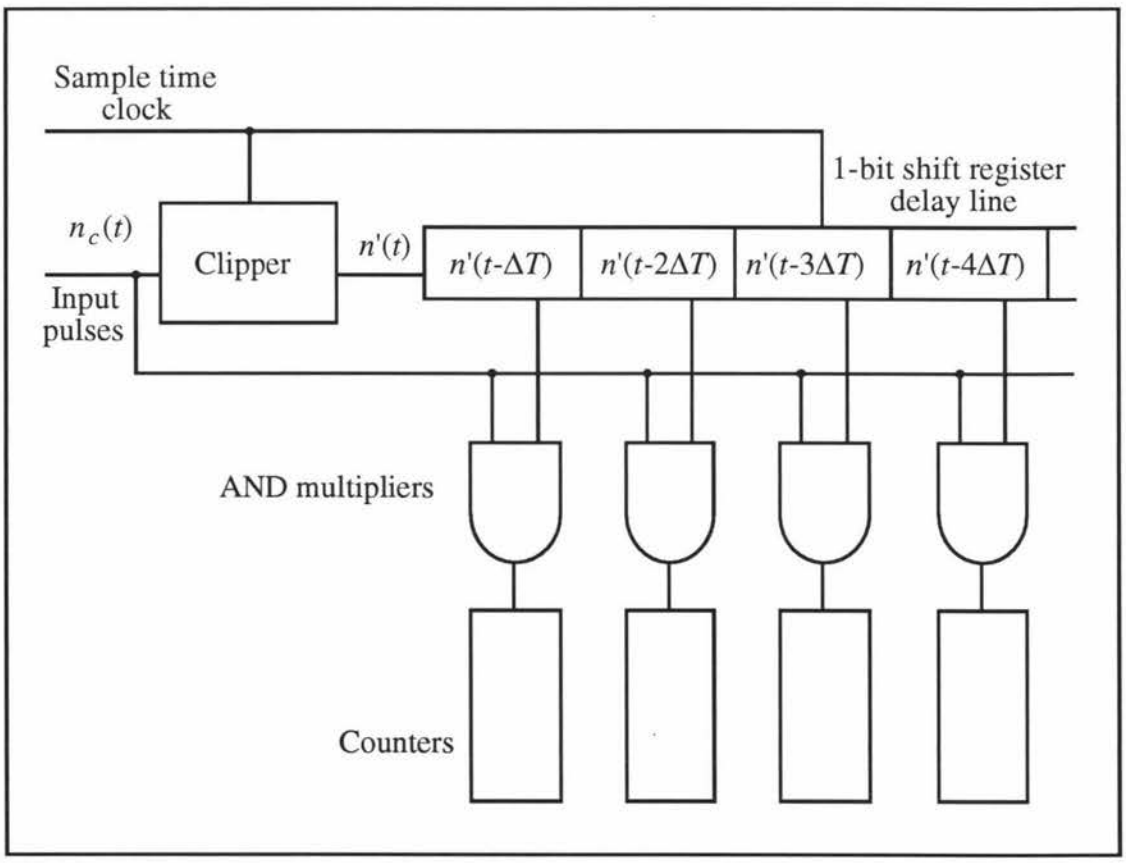

Figure 4.5 Single-clipping correlator

In this kind of correlator (Figure 4.5), input pulses are passed through a clipping gate into a single-bit shift register operating under the control of sample time clock. All input pulses are passed in parallel to a bank of AND gates, which is used to gate the contents of the shift register into a bank of counters. In this manner, because of the necessary restriction to single-bit signals in the delayed input only, each counter accumulates one channel of the $1\times N$-bit correlation function. Additional counters are provided for the monitor channels (number of samples; number of input counts; number of clipped counts). Further circuitry allows for real-time readout for display and storage, selection of a sample time as a multiple of 50 ns, and auxiliary functions such as start and stop, and clearing of the store (bank of counters). The O'Driscoll correlator also included the 'blinker' technique to minimise the effect of dust on the measured intensity correlation function.

The data are counted and sent to the shift register delay line which stores the delayed data. Thus the delayed data can be generated as fast as the direct data for the correlation calculation.

Figure 4.6 shows the data structure in the first 4 channels of the shift register delay line at times t, t+DT, t+2DT, t+3DT.

	Channel 0	Channel 1	Channel 2	Channel 3
t	n(t-ΔT)	n(t-2ΔT)	n(t-3ΔT)	n(t-4ΔT)
t+ΔT	n(t)	n(t-ΔT)	n(t-2ΔT)	n(t-3ΔT)
t+2ΔT	n(t+ΔT)	n(t)	n(t-ΔT)	n(t-2ΔT)
t+3ΔT	n(t+2ΔT)	n(t+ΔT)	n(t)	n(t-ΔT)

Figure 4.6 Data structure for clipping correlator using a shift register

Figure 4.7 shows a general signal analysis system in a dynamic light scatterimg experiment.

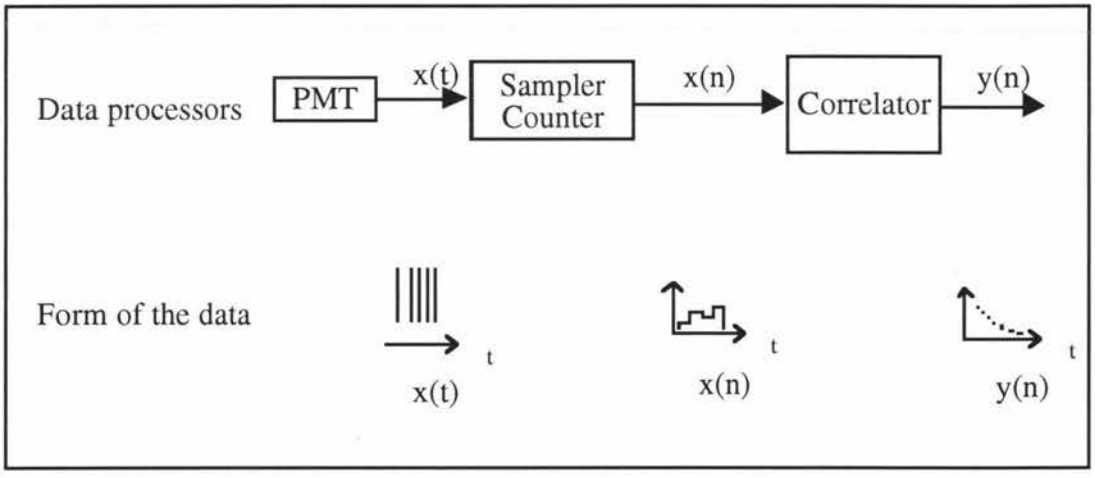

Figure 4.7 General signal processing system.

4.5 Experimental Technique

4.5.1 Apparatus

A schematic diagram of the apparatus used in the dynamic light scattering experiments is shown in Figure 4.8

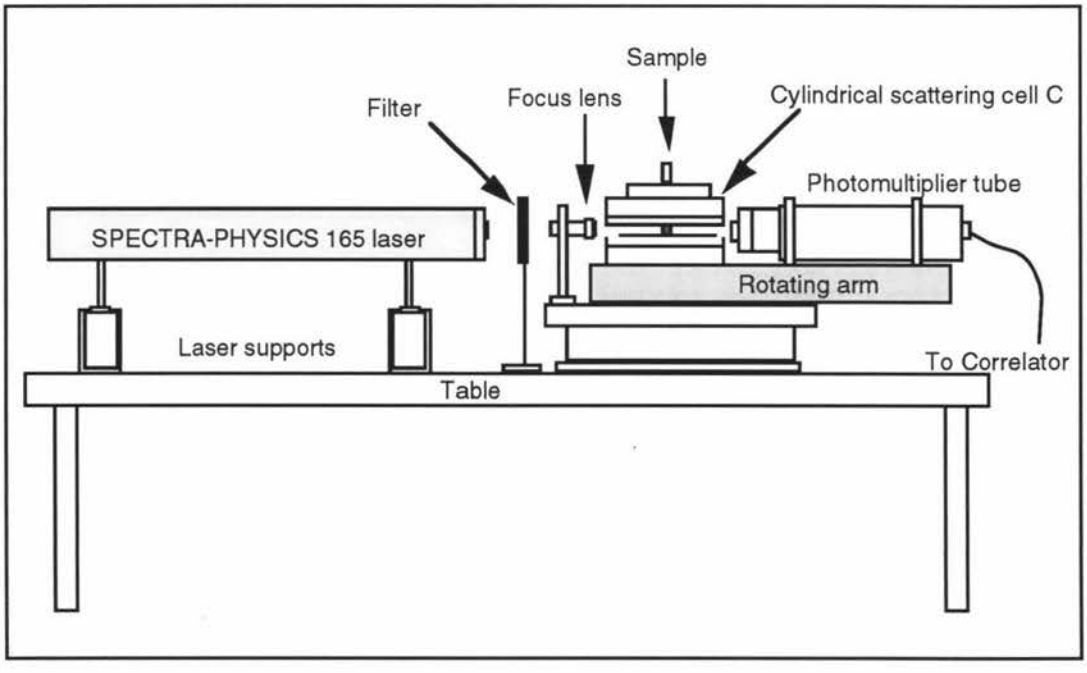

Figure 4.8 Dynamic light scattering apparatus.

The light source used is a Spectra Physics 165 argon laser operating at a wavelength of 488 nm. The output power was reduced to approximately 100 mW using a variable neutral density filter. The beam is weakly focused with a 10 cm focal length lens to give a high intensity in the scattering volume.

The measurements were made with a Malvern Instruments RR102 spectrometer. It consists of a refractive matching bath to reduce unwanted reflections from the glass cells used to contain the samples, this bath also acts as a temperature control bath to maintain the sample at a constant temperature, a spectrometer rotation unit and an ITT FW 130 photomultiplier assembly which also includes collection optics and a pulse preamplifier and discriminator. The collection optics are designed to provide coherent detection of the scattered light while the preamplifier and discriminator produce standardized pulses corresponding to photoelectron detections. The laser and spectrometer are securely located on a massive table supported by foam rubber mounts to give good vibration isolation and stability.

The standardized pulses are processed by a digital correlator (as mentioned earlier). This correlator has 48 correlation channels with an available range of sample times from 0.05 μs to 9.95 x 10^5 μs. Four monitor channels are provided for the normalisation of correlation functions.

The correlator is connected to a Macintosh IIvx computer which is used for remote control of the correlator and data collection and analysis. An Hewlett-Packard Desk Writer and 7470A plotter are connected to the computer to provide printed output and plots of data.

4.5.2 Laser Light Scattering of Samples

Prior to making any measurements, the laser was always allowed to warm up (at least two hours) and the operator must ensure that the laser beam was properly aligned with the optical axis of the spectrometer and the vat containing the refractive index matching fluid was already filled. The filtered sample was then placed in the temperature control bath set at 25°C in the direct path of the laser beam. Appropriate adjustments and attenuation of the beam were carried out when needed in order to maximise count rate and to minimised problems due to the presence of dust particles. The goniometer arm was set so that the photomultiplier collected light scattered through the appropriate angle. The sample was left to equilibrate for at least 20 minutes before data were collected. That would enable any convection currents to dissipate and the dust particles (if any) to settle at either the top or bottom of the sample. Measurements were not usually made at angles higher than 90° because of the low count rates observed at such angles.

Appropriate parameters were selected from the correlator for each sample depending on the behaviour of an oscilloscope trace and the intensity of light scattered. The behaviour of the trace could easily indicate the presence of larger and unwanted particles. Further adjustments of the detector angle and the sample time were made when necessary since the sample time and detector angle are both key factors in obtaining the best time scale of the correlation function. If the sample time is too long then all the relevant decay information is in the first part of the autocorrelation function, whereas if it is too short, not all of the information will be collected. In addition, if the detector angle is too large, there may not be enough signal from the scattered light. The relationship between the detector angle, θ, and the decay time, t_d, is such that

$$t_d \propto \left[\sin^2\left(\frac{\theta}{2}\right)\right]^{-1} \tag{4.32}$$

This relationship shows that the smaller the detector angle, the longer the sample time required.

Several runs were performed on the same sample and the data were then averaged. The number of accumulations per run was determined by the nature of the sample. For weakly scattering samples, it was often advantageous to average many shorter runs rather than accumulating one run over a long period. Runs can be scrutinised before being included in the average and those which are obviously distorted can be excluded. Data showing evidence of an unusually high scattered intensity are rejected by a rejection scheme which is incorporated in the software used for this experiment (Daivis 1989). The rejection scheme discarded the accumulations which varied considerably from the average of the previous runs. Data were then processed by the computer to give plots of the log of the autocorrelation function versus time.

The solutions used for this part were the same solutions used in the ultra centrifuge studies but special techniques were used to prepare the samples for light scattering measurements (refer to chapter 3). This is due to fact that light scattering results could be affected by the presence of dust whereas in the ultra centrifuge studies dust particles always sediment very much faster than the particles of interest and so do not interfere with data collection.

4.6 Results and Discussion

4.6.1 PMMA / PS / Thiophenol

4.6.1.1 Variation of D_I with the total polymer concentration, c.

The correlation functions measured in this work compromised a single relaxation mode, suggesting that the PS-thiophenol pair is a sufficiently good approximation to an isorefractive system to give single exponential behaviour at low PS concentrations and the variation of the decay rate with scattering angle indicated that it was due to a simple diffusive process.

The value of D_I for each solution was obtained from the decay rate. The values of D_I obtained in these experiments are presented in Table 5.2 and are plotted in Figure 4.9 as log D_I against log c where c is the total polymer concentration expressed in gram per gram of solvent. The value of D_I decreases as the polymer concentration increases.

Figure 4.9 also shows a comparision of the interpenetration diffusion coefficients obtained from this study with those obtained by Nemoto et al. [30] from similar solutions. The uncertainties in the measurements reported here are indicated by the size of the plot symbol. The interpenetration diffusion coefficients measured in this work are in good agreement with those reported by Nemoto et al. [30] thus confirming the theoretical prediction that the interpenetration diffusion coefficients should be very nearly equal in these two systems.

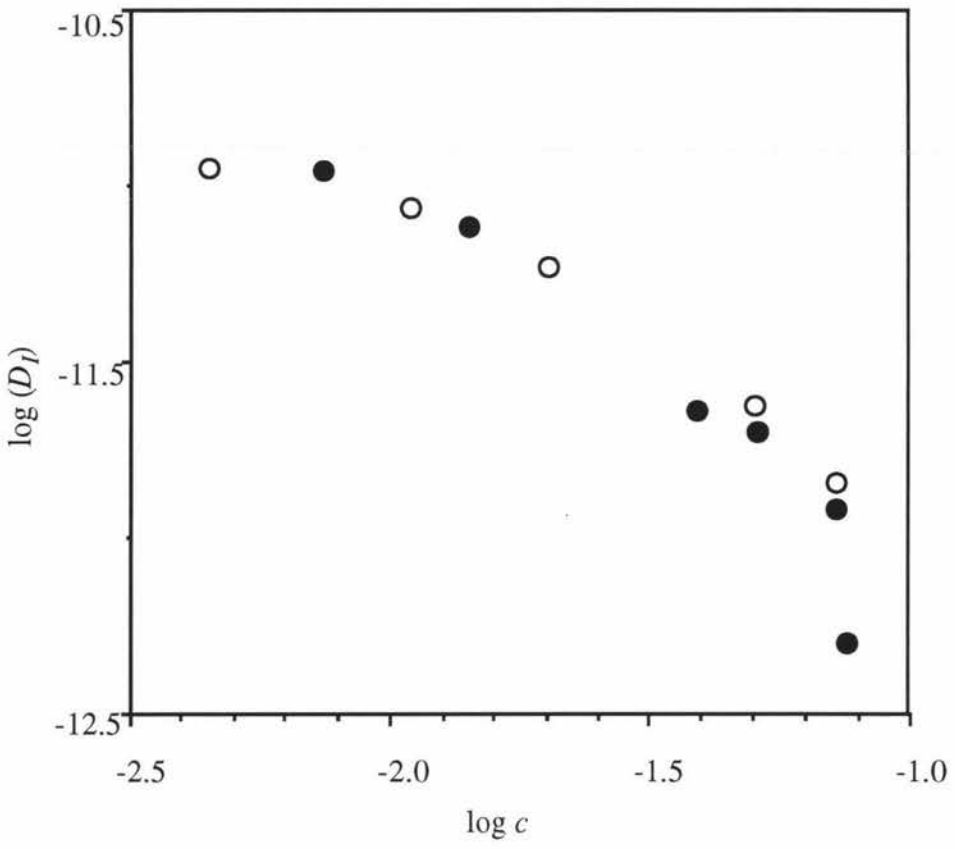

Figure 4.9 Variation of dynamic light scattering determined diffusion coefficient, D_I, with total polymer concentration, c, to logarithmic scales. Diffusion coefficients expressed in $m^2\ s^{-1}$. ● this work. ○ Nemoto et al., see Table 2.1

Additional non-diffusive slower decays were manifest in the auto correlation function of the scattered light at the largest polymer concentration studied here. This behaviour has been observed previously in ternary polymer solutions which are close to phase separation [46], and has been ascribed to persistent slow hydrodynamic reorganisations of the solution. Daivis [17] have shown that if phase separation is caused by the solvent being of unequal quality for the two polymers then the Borsali-Benmouna theory fails. However, if phase separation is caused by polymer-polymer incompatibility, as is believed to be the case here, then the Borsali-Benmouna theory is valid to polymer concentrations close to phase separation and D_I is expected to gradually reduce to zero as the polymer concentration is increased. A significant decrease in the value of D_I is observed for the solution with the largest polymer concentration, confirming that D_I decreases as phase separation is approached. This solution was not studied using ultra centrifugation and attempts to form ternary solutions at greater concentrations failed.

4.6.1.2 Variation of D_I with the temperature, T.

The dependence of D_I on temperature was also investigated on the solution with the largest polymer concentration in which the PMMA volume fraction was 0.00092 and the total polymer volume fraction was 0.080. This solution was very close to phase separation at 25°C. The temperature of the solution was lowered and then the respective D_I was measured. The values of D_I obtained from these measurements are plotted in Figure 4.10 as log D_I against temperature.

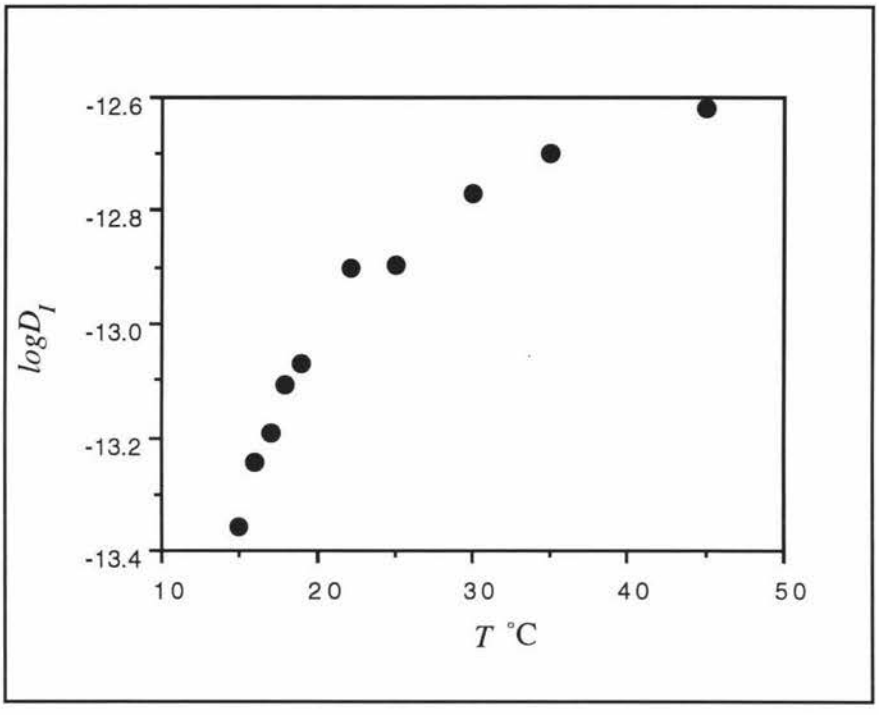

Figure 4.10 Variation of D_I with temperature. Diffusion coefficients expressed in $m^2\ s^{-1}$

D_I decreases as the temperature is lowered as expected since phase separation could be induced by lowering the solution temperature. This result supports the Benmouna et al [4] theory of DLS from case A type ternary polymer solutions close to phase separation in which $q\xi$ was always less than unity.

These data have been represented in Figure 4.11 where the correlation length ξ_d (defined as $kT/6\pi\eta D$) is plotted against ε ($\varepsilon = (T - T_c)/T$) to logarithmic scales.

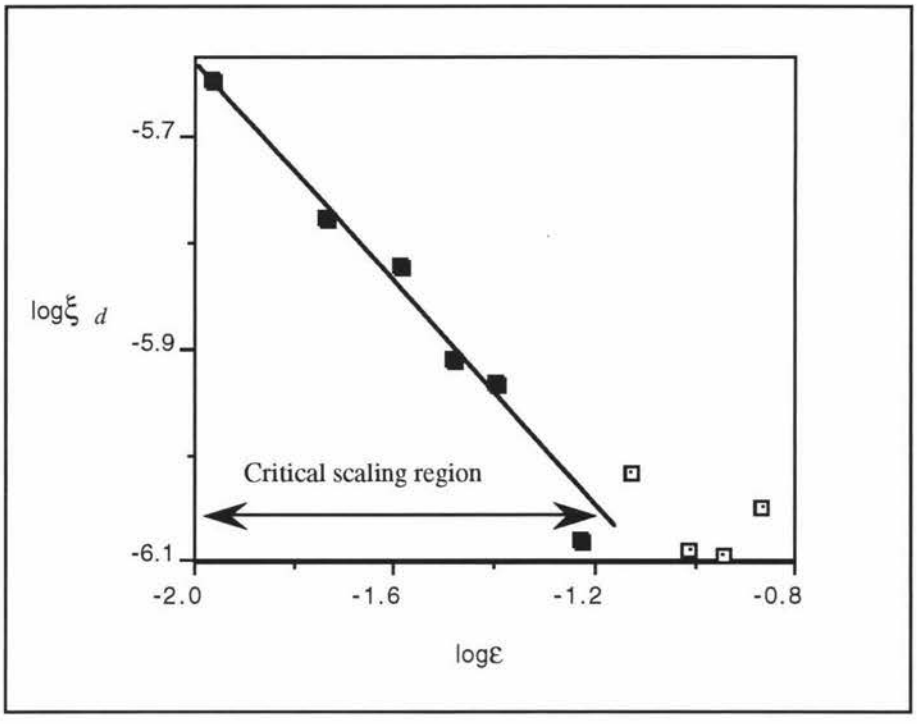

Figure 4.11 Graph of log ξ_d vs log ε

Taking the critical temperature T_c to be 13°C, for this solution (cloud point), the linear scaling region yields the correlation length critical exponent, n, to be 0.60 (±0.07). This is to be compared with the mean field theory, three dimensional Ising and Fisher renormalisation values of 0.50, 0.63 and 0.71 respectively. The scaling region is too narrow and the thermal stability of the experiment was too poor for a more precise determination to be obtained. However, it should be noted that Seils et al [42] were unable to quote a value for n from their DLS experiment on a similar system, although they did obtain the value 0.57 from static light scattering observations (no uncertainty stated). Migashitu et al (1994) have also used static light scattering to obtain the value 0.64±0.02 for n for similar ternary polymer solutions.

4.6.2 PVME / PS / Thiophenol

The solvent thiophenol is so little used that there is no information available regarding its 'quality'. That is, whether it is a good solvent for PS or PVME or for both. Dynamic light scattering could indicate if the solvent were of very different quality for the two polymers.

The measured diffusion coefficients of the PVME in ternary solutions with polystyrene and thiophenol have been normalised to 30°C so that the values can be compared with measurements made with other solvents. The polymer concentrations have been expressed as volumes fractions for the same reason. The polymer concentrations, the PVME volume fraction and the diffusion coefficients are shown in Table 4.1.

Table 4.1 Diffusion Coefficients of PVME.

Volume fraction (g / ml)	***x*** (mass of PVME / mass of polymers)	***D*** ($\times 10^{-12}$ m^2 s^{-1})
0.024	0.197	29.51
0.080	0.186	4.59
0.120	0.199	1.54
0.169	0.222	1.00
0.210	0.222	0.44
0.265	0.222	0.22

The variation of D with polymer volume fraction for these solutions is compared with the variations for an equally good solvent (toluene) [16] an equally poor solvent (tetrachloroethylene) [13], and a solvent of unequal quality (carbon tetrachloride) [13] in Figure 4.12.

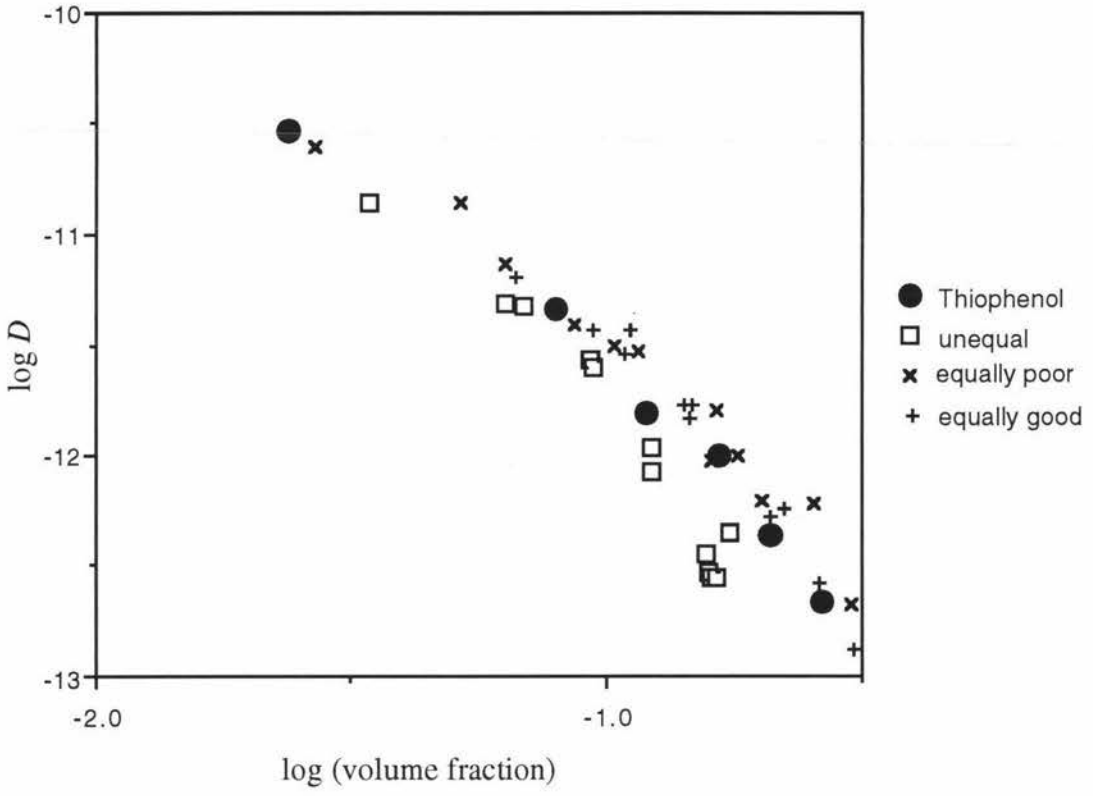

Figure 4.12 Variation of D with PVME volume fraction.

Daivis [16] has shown that the values of diffusion coefficient obtained for solutions formed with an equally good solvent are indistinguishable from the PVME self diffusion coefficient obtained from pulsed field gradient nmr studies.

Clark [13] has shown that data collected from solutions formed with an equally poor solvent are also in agreement with the PVME self diffusion coefficient. However, data collected from solutions formed with a solvent of unequal quality show a systematic reduction of the dls determined diffusion coefficient compared with the self diffusion coefficient of the PVME.

The data collected in this work are in approximate agreement with Daivis' observations of the PVME self diffusion coefficient which would seem to indicate that thiophenol is an approximately equal quality solvent for the two polymers, though whether equally good or equally poor cannot be ascertained from this work. Certainly the solvent does not appear to be as unequal a solvent as carbon tetrachloride

The data cannot be used to determined the polymer-polymer interaction parameter because the interpenetration diffusion coefficient is indistinguishable from the PVME self diffusion coefficient.

Chapter 5
Ultracentrifuge Studies

5.1 Introduction

Ultra centrifugation is a technique for measuring the movement or redistribution of sedimenting particles under the action of high centrifugal forces. This technique can be used to determine various molecular parameters, including sedimentation coefficients, diffusion coefficients, molecular weights, particle sizes and shapes and partial specific volumes.

The ultracentrifuge consists of a steel (or titanium) rotor several centimeters in diameter which is spun at very high speed in a very low pressure chamber (in order to minimise thermal effects). The rotor is driven electrically at constant speed. The small sector shaped cell containing the solution being studied is held within the rotor near its periphery. Concentration gradients in the cell are determined optically by using a beam of light travelling in a direction parallel to the axis of rotation and perpendicular to the cell, the beam being intercepted by the cell at each rotation. Refraction of the beam passing through different portions of the cell is determined by the use of Schlieren optics, which affords a simple method to convert refractive index gradients to concentration gradients along the direction of sedimentation within the cell.

Ultracentrifuge studies generally conform to one of three ultracentrifugal methods: the sedimentation velocity method, which studies the sedimentation rate of molecules; the sedimentation equilibrium method, which studies the concentration distribution of molecules at equilibrium positions; and the approach to equilibrium method, which studies the concentration distribution of molecules at early stages of an equilibrium or a velocity run.

The sedimentation velocity method was used in this study to measure the sedimentation and one of the diffusion coefficients of PMMA which was dissolved with polystyrene in thiophenol. Preparation of this ternary solution has been discussed in chapter 3. An analysis of the sedimentation velocity method is given below.

5.2 Sedimentation Velocity Method

In a sedimentation velocity study the rotor is operated at high angular speeds so the solute molecules in the solution are subjected to high centrifugal forces. If the solute has a greater density than the solvent, then it migrates radially (outwards). The solute molecules are said to "sediment" towards the "outerside" of the cell at appreciable rates. In a single-component, non-interacting system this transport of molecules produces a region in the cell containing only solvent (supernatant) and a region in the cell where the polymer concentration is uniform. This region of uniform concentration is called the plateau region. Between the supernatant and the plateau region is a transition zone, called the boundary, in which the concentration varies with distance from the axis of rotation. See Figure 5.1. The migration of this boundary corresponds to the migration of the solute molecules in the plateau region.

Although the rate of migration of individual molecules under the influence of the centrifugal field is desired, no direct techniques are available which permit direct viewing of individual molecules as they traverse the cell. Most sedimentation velocity studies, rely upon an optical system to provide, in an indirect manner, a measure of the transport of the solute materials across a surface. Although it is by no means obvious, it can be shown by means of a differential equation (continuity equation) that the movement of the boundary between the supernant and the plateau region usually provides a measure of the migration rate of individual molecules in the plateau region.

The continuity equation, which is basically used by almost all ultracentrifugal measurements, is actually a statement of the conservation of mass. In its derivation, the continuity equation provides a definition of the sedimentation coefficient. For a sedimentation velocity experiment in which the concentration at the meniscus becomes equal to zero, this equation gives detailed information concerning the shape of the boundary. In addition, the continuity equation can be used to describe the dilution of the contents of the cell as a function of time and, when integrated with appropriate data, can also provide a description of solute distribution as a function of distance in the cell. The appropriate form of the continuity equation, originally derived by Lamm (1929) is

$$\frac{\partial c}{\partial t} = \frac{1}{r}\frac{\partial}{\partial r}\left[r\left(D\frac{\partial c}{\partial r} - cs\omega^2 \right)\right] \tag{5.1}$$

where r is the distance from the axis of rotation in cm, D is the diffusion coefficient, c is the concentration in $g.ml^{-1}$, s is the sedimentation coefficient, ω is the angular velocity, and t is the time in minutes.

If the solute is sufficiently dilute, one can assume that the sedimentation and diffusion coefficients are independent of concentration and therefore of the position in the cell. In such a case, equation (5.1) can be written as

$$\frac{\partial c}{\partial t} = D\left[\frac{\partial^2 c}{\partial r^2} + \frac{1}{r}\frac{\partial c}{\partial r}\right] - s\omega^2\left[r\frac{\partial c}{\partial r} + 2c\right] \tag{5.2}$$

In formulating the continuity equation, it is necessary to describe the transport of material across the surface under the influence of the centrifugal field. Transport of material is the product of a concentration at a given surface, the area of that surface, and the velocity with which the molecules cross that surface. Since the velocity of sedimentation at a point in the cell can be express as the velocity per unit field (or the sedimentation coefficient, s, times the magnitude of the centrifugal field, $\omega^2 r$), the sedimentation coefficient can be defined as follows

$$s = \frac{dr/dt}{\omega^2 r} \tag{5.3}$$

The sedimentation coefficient is thus a measure of the transport of material across the surface of a cell under the influence of a centrifugal field.

It is important to note that concentration changes continually during the run. This continual change in concentration, commonly called radial dilution, is a direct consequence of the movement of the molecules in a radial direction in a sector-shaped cell and of the inhomogeneity of the centrifugal field. The concentration (as a function of time) varies inversely with the square of the distance of the boundary from the axis of rotation. Moreover, it should be noted that the boundary itself represents a transition zone in which the concentration varies from zero in the supernatant region to some constant value in the plateau region. Although the movement of the boundary provides a measure of the sedimentation coefficient of the molecules in the plateau region, the shape of the boundary is markedly affected by concentration changes across it.

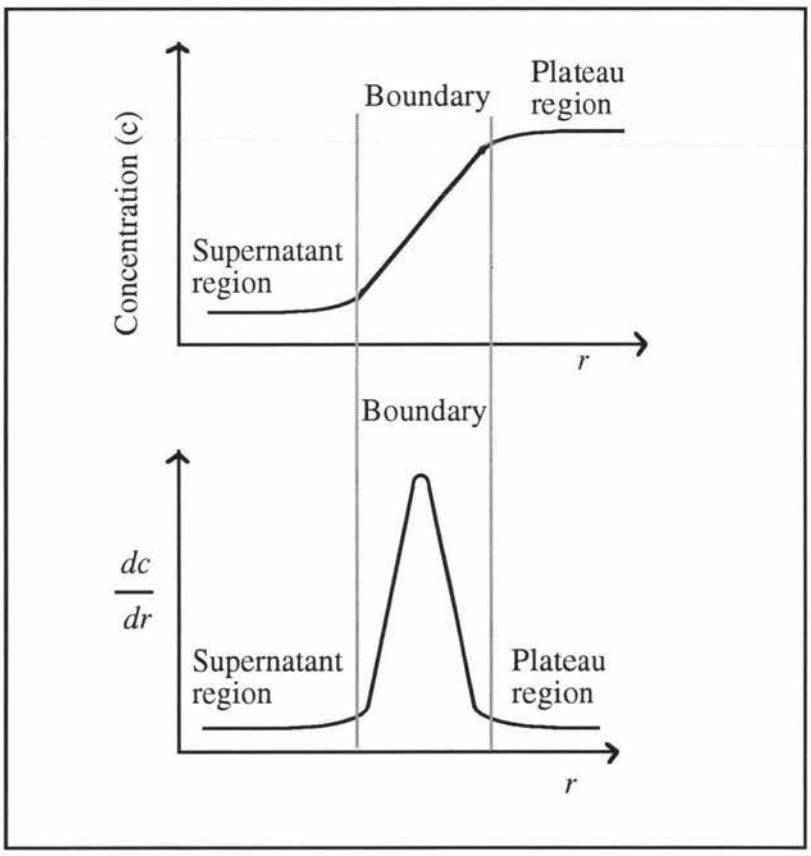

Figure 5.1 Plots of the concentration and the rate of change of concentration against the distance from the axis of rotation.

A plot of concentration as a function of distance from the axis of rotation shows the position of the boundary at a given time (see Figure 5.1). A plot of the rate of change of concentration as a function of distance from the axis of rotation not only shows the position of the boundary but also shows the width and the midpoint of the boundary more clearly (refer to Figure 5.1). This rate of change of concentration at the boundary is called the concentration gradient. The area beneath each peak is proportional to the concentration of the solute. Thus the plot of the concentration gradient can be used to calculate both the concentration and the rate of movement of solute molecules during centrifugation.

A Schlieren optical system is used to locate the position of the boundary since it provides an image which represents the rate of change of concentration as a function of distance from the axis of rotation. The boundary appears as a peak in the Schlieren pattern and is often refered to as the "Schlieren peak". The regions of uniform concentration create the baseline which defines the level of the pattern representing the zero solute concentration gradient (see Figure 5.2). Photographs of the Schlieren peak can be taken at appropriate intervals using the Schlieren optical system.

In most substances the movement of the maximum ordinate of the boundary can be used as an accurate indicator of individual particle movement in the plateau region. This provides the basis for the common practice of measuring sedimentation coefficients from the maximum ordinate boundary positions. The peak broadens as it migrates from the meniscus due to mutual diffusion of the solute and solvent hence the maximum height of the peak as well as the area under it decreases. Refer to Figure 5.3.

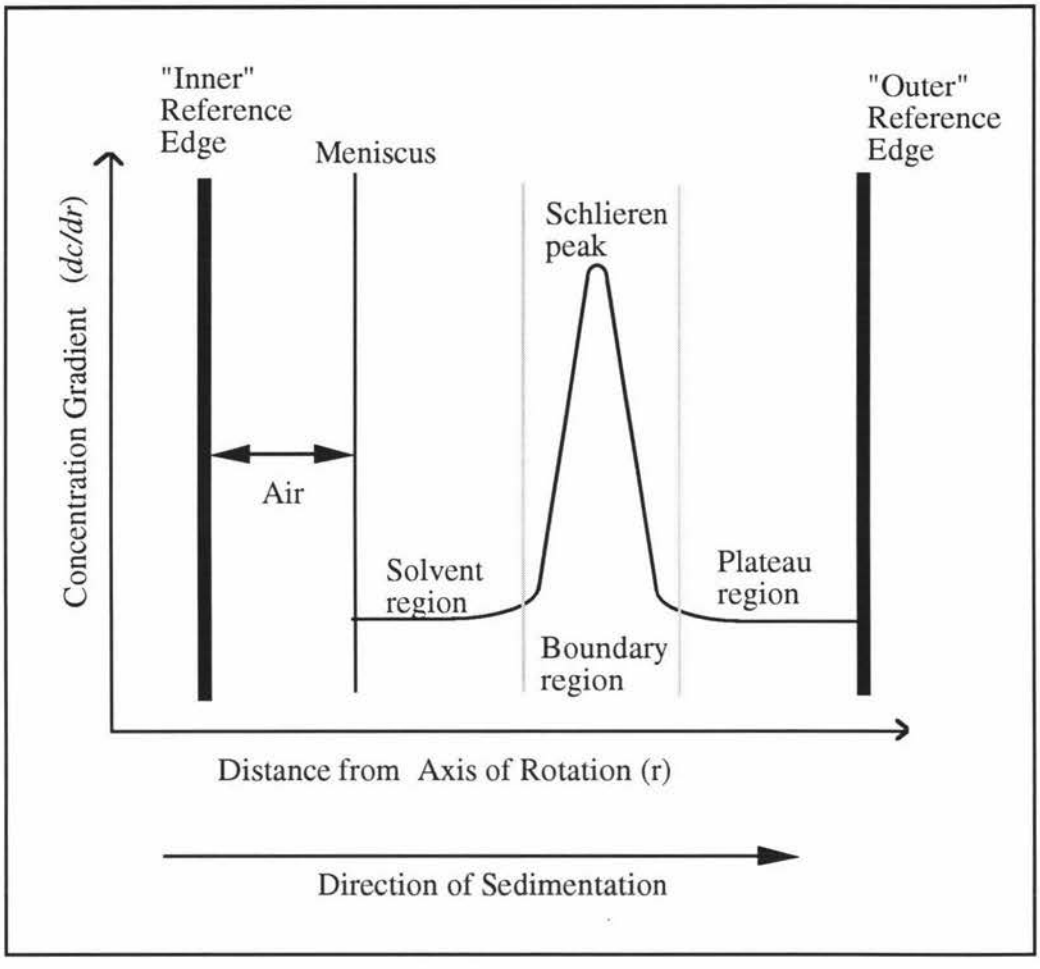

Figure 5.2 Typical Schlieren Pattern.

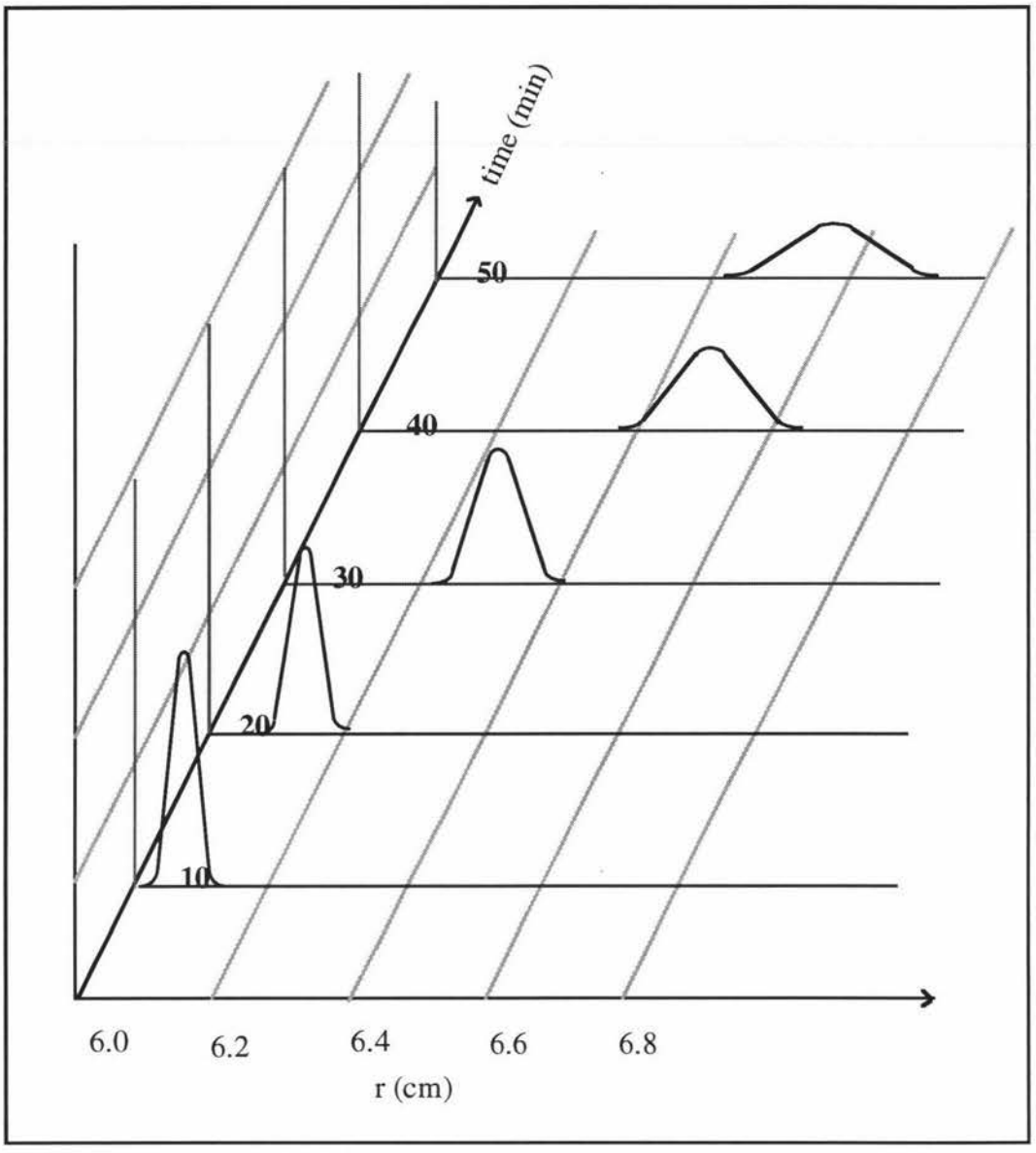

Figure 5.3 Plot of the Schlieren Peak against time and distance from axis of rotation.

5.2.1 Measurements of Sedimentation Coefficients

There are various methods in ultracentrifuge studies which can be used to measure the sedimentation coefficient of the solute under investigation. The method used in this study is known as the "moving boundary method". In this method, the sedimentation coefficients are generally evaluated from the slope of a plot of the natural logrithm of the boundary position with time. This approach to sedimentation coefficient is based on equation (5.3), which can be written in the alternative form

$$s = \frac{1}{\omega^2} d\left(\frac{\ln r}{dt}\right) \tag{5.4}$$

This equation is valid provided the temperature is constant during the run. If the temperature were to vary appreciably the equation would have to be refined in the manner described in Oncley (1941), Cecil and Ogston (1948), Kegeles and Gutter (1951) and Schwert (1954). Such complications were avoided in this work by ensuring that the temperature was maintained at 25.0 ± 0.1°C.

When measurements are very precise, a plot of log r versus t will provide a curved line rather than a straight line. The non-linear relationship of the experimental points is clearly a result of both radial dilution and the dependence of the sedimentation coefficient upon concentration. In other words, the dilution of the contents of the cell with time produces a concomitant change in the sedimentation coefficient with time and thus produces an upward curvature in the plot of log r versus t. But with some materials (polymers, for example) concentration changes are so minimal that the experimental plot of log r versus t produces an essentially straight line. However, for the most precise results, allowances should be made to correct for the dilution effect.

5.3 Experimental Technique

The ultracentrifuge used was a Beckman model E analytical ultracentrifuge with an An-H rotor (titanium) operating at 56 000 rpm over long time scales. The current to the motor was constantly adjusted to maintain it at 12 amps so that the rotor suffered constant acceleration until it reached 56 000 rpm. The current was then dropped to 4 amps for the rest of the run to ensure that the rotor spun at the constant angular speed of 56 000 rpm. The speed of the ultracentrifuge was checked during each run using the odometer readings. Due to the finite time taken to reach the running angular speed, "time zero" is conventionally taken as the time at which the angular velocity is two thirds of the final value. The sample was loaded into a 2.5° single sector aluminium cell and properly placed into the rotor with an appropriate counterbalance. Proper alignment of the cell in the rotor is a very important factor in achieving accurate results in this kind of study. The counterbalance was always kept lighter than that of the filled cell (up to 0.5g lighter) to ensure that if there were any leakage from the cell the difference between the mass of the cell and that of the counterbalance would narrow instead of widen. The temperature of the rotor was maintained at 25.0 ± 0.1°C by the Rotor Temperature Indicator and Controller (RTIC) unit.

The Schlieren optical system was used for viewing and analysing the refractive index gradient in the cell. It produced a concentration gradient profile curve from which the position, width and midpoint of the boundary could be readily obtained. Light of

wavelength 546.1 nm was used and the analyser angle was set to 60°. The progress of each ultracentrifuge run was monitored visually to check for signs of cell leakage and also to take photographs of the Schlieren profile.

Kodak photographic glass plates were used and were preloaded into plate holders in a dark room before each run. Photographic glass plates were used because they do not shrink during the developing process and thus preserve the details needed for this study. Plate holders were loaded with the emulsion side facing the slide cover. The emulsion side was identified by touch: two fingers were moisten and pressed one on each side of the plate at the corner, the emulsion side became sticky. Five photographs were taken on each plate and each photograph had an exposure time of 40 seconds. The first photograph was always taken at "time zero". Plates were developed for five minutes in Kodak D-19 developer, rinsed in a stop-bath for one minute and then immersed in a Kodak fixer for four minutes. Photographic processing was carried out in complete darkness, using cylinders for the solutions which were little larger than the glass plates. Plates were then washed in running tap water for 20 to 30 minutes and then dried in air.

5.4 Results and Discussion

5.4(a) PMMA / PS /Thiophenol

5.4.1 Analysis of the Photographic Plates

The photographic plates were analysed using a Nikon 6CT2 Profile Projector. Measurements of the radial positions of the images were relative to the inner reference edge of the counterbalance. This edge was taken as 5.70 cm from the center of the rotor since the titanium rotor suffered negligible distortion during ultracentrifugation. Each plate was placed on the comparator carriage with the emulsion side up and oriented so that the images as seen on the screen were right side up and the imaginary center of rotation was to the left when facing the comparator. The plate was rotated so that the meniscus image was exactly parallel to the crosshair of the view screen as the plate was moved up and down across the view. The crosshair was then moved to the maximum ordinate of the Schlieren peak (boundary position). This distance was then divided by a previously determined magnification factor before adding to the reference distance of 5.70 cm to obtain the actual radial distance.

The magnification factor was obtained by dividing the distance between the two reference edges of the counterbalance measured from the Schlieren image by the distance measured from the counterbalanced itself. Both distances were measured using the Nikon comparator.

5.4.2 Sedimentation Coefficient

A single peak was observed in the photographs of the Schlieren pattern. This shows that the polystyrene did not sediment but constituted an "effective solvent" with thiophenol through which the PMMA molecules sedimented and diffused. The sedimentation coefficient, *s*, of PMMA for each solution was determined from the slope of a graph of ln *r* against time *t* using equation (5.4). The graph used to obtain the sedimentation coefficient of the solution with total polymer concentration of 0.012g/g is shown in Figure 5.4.

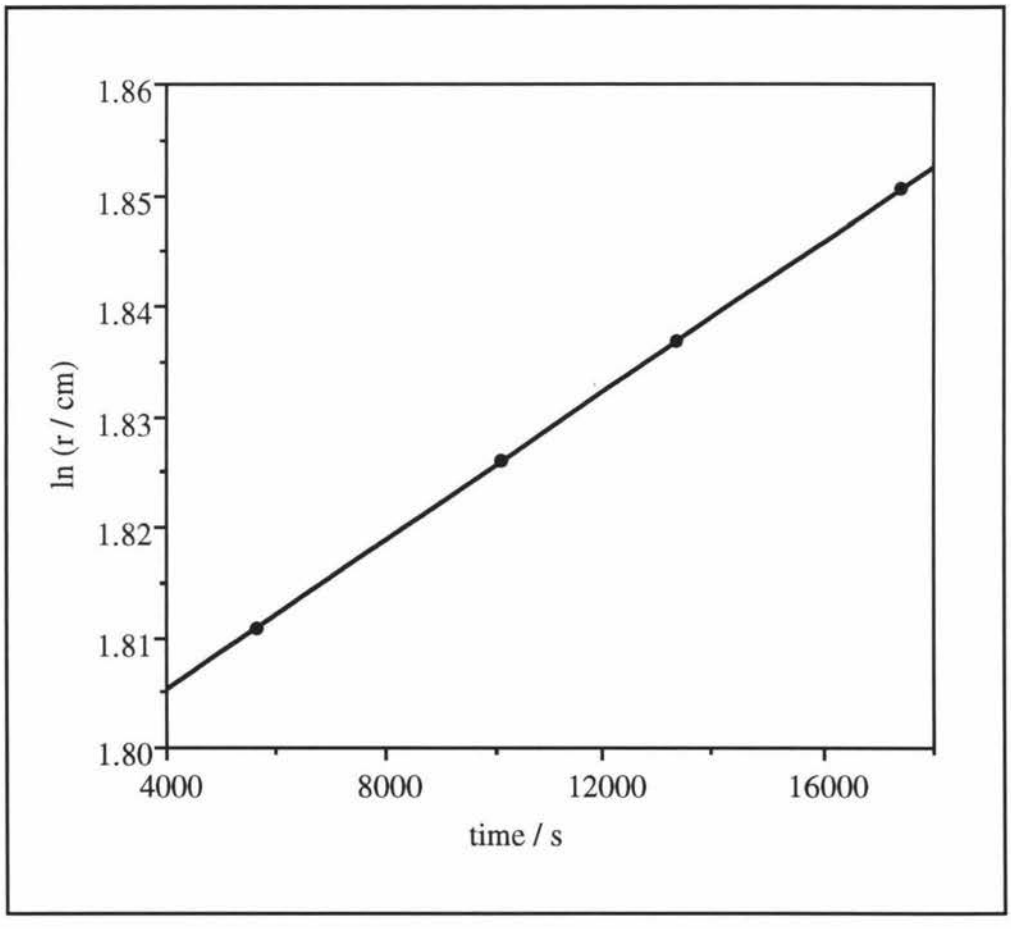

Figure 5.4. Plot of ln r against time for data which were collected from the solution with total polymer concentration of 0.012 g/g. The sedimentation coefficient caculated from the slope is 0.98×10^{-13} s.

The values of s obtained in these experiments are plotted in Figure 5.5 as log s against log c where c is the total polymer concentration expressed in gram per gram of solvent. The graph shows that s dereases monotonically with increasing concentration of polystyrene. This decrease in the sedimentation coefficient is at least partly due to the frictional effect between the molecules which increases as they get closer together. Note that the concentration of PMMA was kept constant at approximately 0.001g/g.

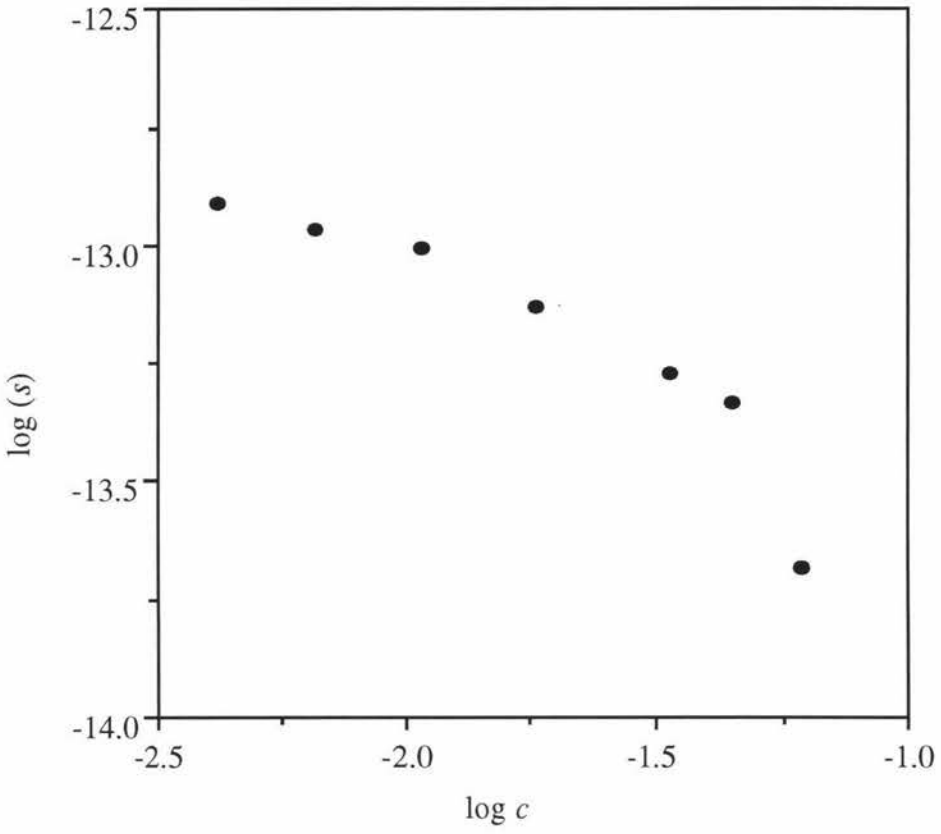

Figure 5.5 Variation of sedimentation coefficient, s, with total polymer concentration, c, to logrithmic scales.

Figure 5.6 shows a comparision of the sedimentation coefficients obtained from this study with those obtained by Nemoto et al. [30] from similar solutions. The uncertainties in the measurements reported here are indicated by the size of the plot symbol. The sedimentation coefficients measured in this work are in good agreement with those reported by Nemoto et al. [30] thus confirming the theoretical prediction that the sedimentation coefficients should be very nearly equal in these two systems.

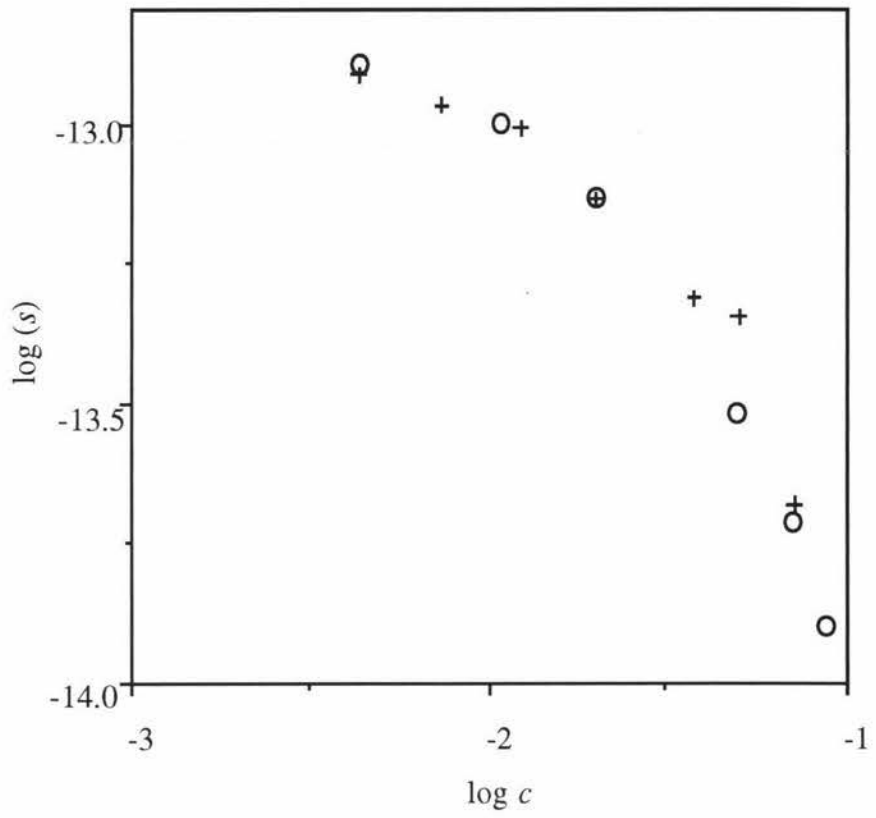

Figure 5.6 Variation of sedimentation coefficient, s, with total polymer concentration, c, to logarithmic scales. + this work. O Nemotot et al., see Table 2.1.

5.4.3 Diffusion Coefficient

The photographic plates used to measure the sedimentation coefficient were also used to determine the diffusion coefficient by measuring the height (maximum) to area ratio of the Schlieren peaks. The area under each peak was measured using a Nikon comparator. A detail describtion of this procedure has been presented in chapter 2. The area under the Schlieren peaks decreased as they moved across the cell due to decreasing concentration in the plateau region during the course of the run.

The area under each peak was then divided by the maximum peak height and these height to area ratio data were then used to calculate the diffusion coefficient, D from equation (2.14) by plotting the right hand side against the left, lines through the origin were obtained and D was obtained from the square of the initial slope. Straight line graphs enabled D to be determined with little uncertainty, however some data yielded slightly curved lines causing the uncertainties in D to be greater. A typical linear graph is shown in figure 5.7. A detail description of equation (2.14) has been given in chapter 2.

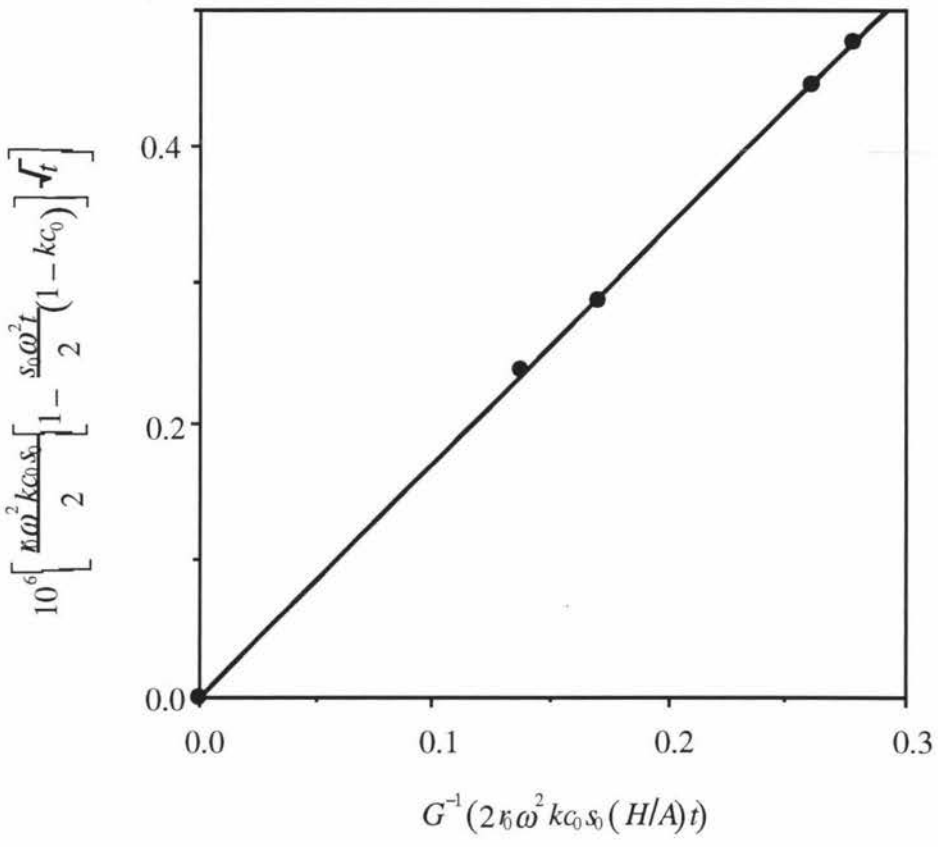

Figure 5.7 Graph of $\sqrt{D}$ times the right hand side of equation (2.14) plotted against the arqument of G. The graph is expected to be linear with slope $\sqrt{D}$. The data were collected from the solution with total polymer concentration 0.0395 g g^{-1}

The values of D obtained in these experiments are plotted in Figure 5.8 as log D against log c where c is the total polymer concentration expressed in gram per gram of solvent. The graph shows that D dereases monotonically with increasing concentration of polystyrene.

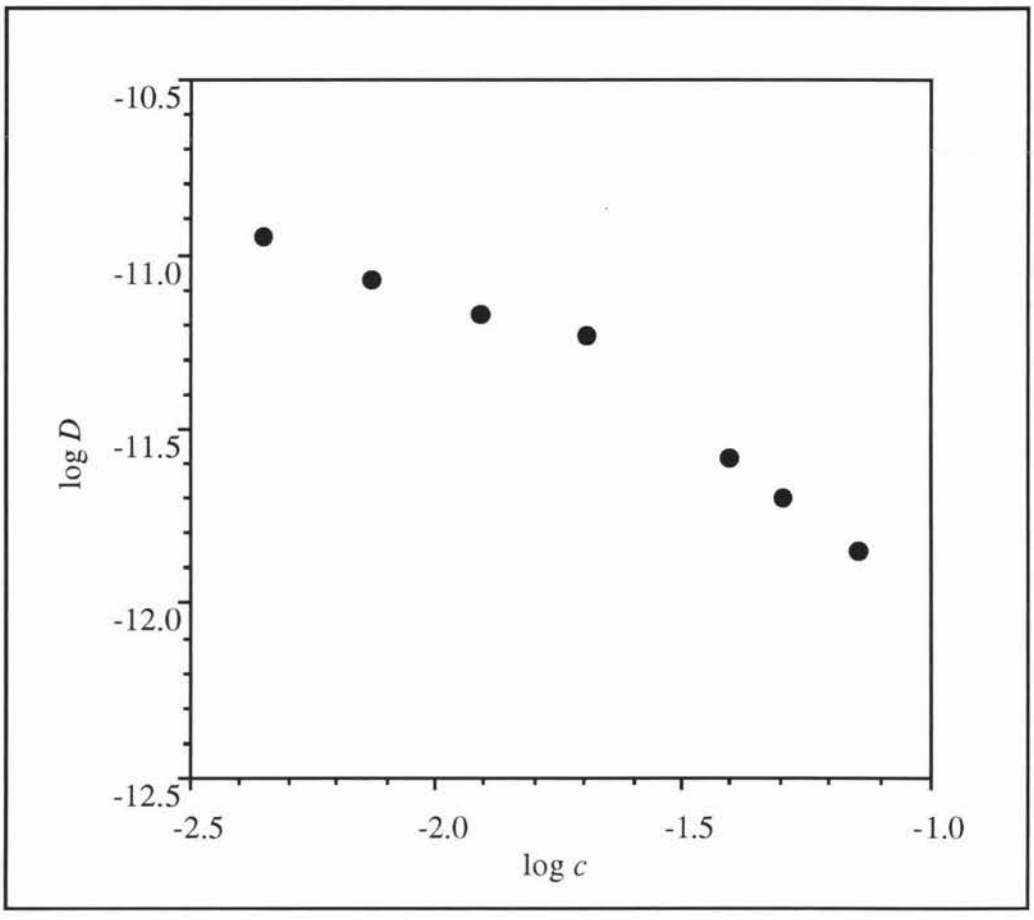

Figure 5.8 Variation of diffusion coefficients, D, with total polymer concentration, c, to logrithmic scales.

Table 5.1 contains the sedimentation coefficient and diffusion coefficient for each sample obtained from these experiments. The concentration given is the total polymer concentration expressed in gram per gram of solvent.

Table 5.1 Sedimentation and Diffusion Coefficients of PMMA.

Concentrations (g/g)	***s*** ($\times 10^{-13}$ s)	***D*** ($\times 10^{-12}$ m^2 s^{-1})
0.00442	1.230 ± 0.006	11 ± 3
0.00743	1.079 ± 0.004	8 ± 1
0.01232	0.98 ± 0.01	6.8 ± 0.5
0.02017	0.74 ± 0.01	5.9 ± 0.8
0.03951	0.534 ± 0.005	2.6 ± 0.3
0.05093	0.461 ± 0.002	2.0 ± 0.4
0.07199	0.207 ± 0.004	1.4 ± 0.8

5.4.4 Comparision of Diffusion Coefficients obtained from Dynamic Light Scattering and Ultra Centrifugation

Table 5.2 Comparision of the diffusion coefficients determined from the light scattering studies (D_I) and those from the ultra centrifugation studies (D).

Concentrations (g/g)	D_I ($\times 10^{-12}$ m^2 s^{-1})	D ($\times 10^{-12}$ m^2 s^{-1})
0.00442		11 ± 3
0.00743	11.0	8 ± 1
0.01232		6.8 ± 0.5
0.01409	7.65	
0.02017		5.9 ± 0.8
0.03951	2.3	2.6 ± 0.3
0.05093	2.0	2.0 ± 0.4
0.07199	1.2	1.4 ± 0.8
0.07550	0.5	

The comparision of the values of D and D_I is also shown in Figure 5.9. The uncertainties in D_I values are represented by the size of the plot symbol, the uncertainties in the ultracentrifuge determination of D are represented by error bars where appropriate. These uncertainties could be reduced if more determinations of H/A were available for each sample.

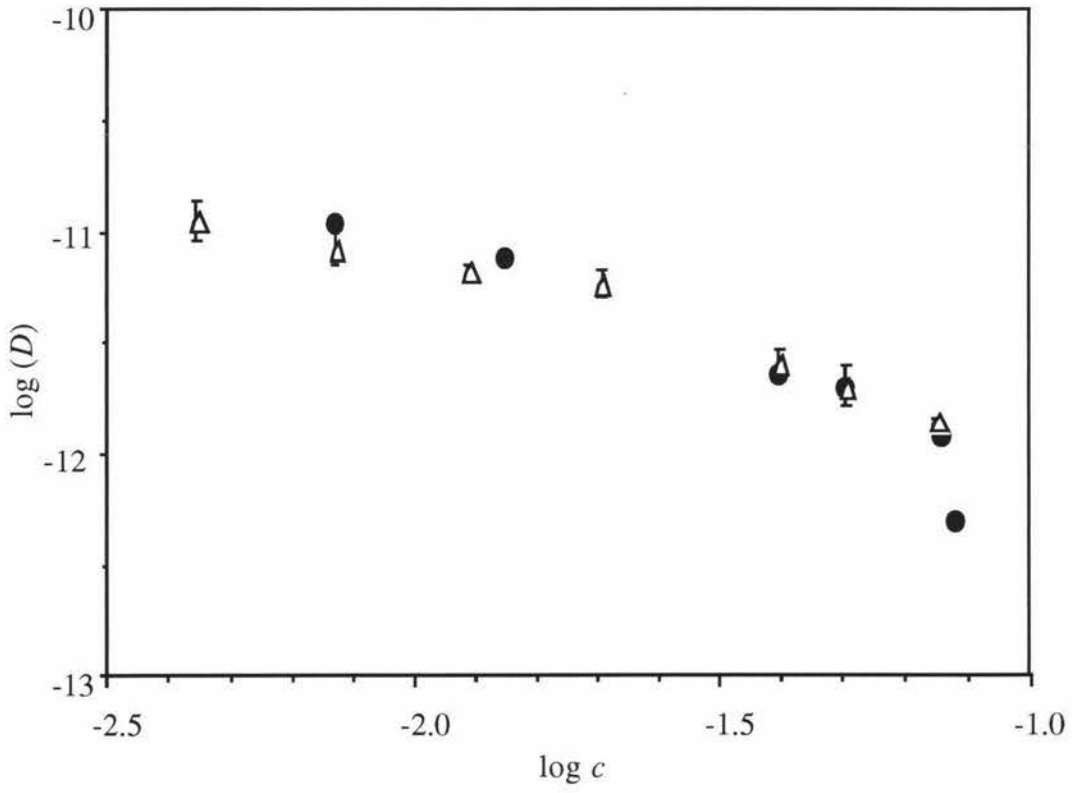

Figure 5.9 Variation of dynamic light scattering determined, D_I, and the ultra centrifugation determined, D, with total polymer concentration, c, to logarithmic scales. Diffusion coefficients expressed in $m^2\ s^{-1}$. ● D_I. Δ D.

There is very good agreement between the values of D obtained from the sedimentation studies and the values of D_I obtained from the dynamic light scattering studies supporting the assumption that the theory of ultra centrifugation for binary solutions can be extended to ternary polymer solutions of the kind described here. One can say that the diffusion coefficient obtained from the ultracentrifugation studies is the same with the diffusion coefficient obtained from the light scattering studies when experimental errors are taken into account.

5.4 (b) PVME / PS / Thiophenol

There were no results obtained from this system. The solution phase separated essentially into two binary solutions, one with PVME and the other with polystyrene. Hence no boundary was visible and no ultracentrifuge observations were possible. It is likely that the ternary solution was so close to phase separation that the centrifugal forces were sufficient to initiate phase separation. PVME and polystyrene are compatible in the melt,

so one suspects that the incompatibility of the ternary solutions formed with thiophenol must be due to the unequal quality of the solvent for the two polymers. If this were so, it is surprising that the dynamic light scattering observations on the same solutions did not indicate that the solvent was of unequal quality. Clearly dynamic light scattering observations are not a sensitive indicator of solvent quality.

Chapter 6
Conclusion

6.1 PMMA / PS / Thiophenol system

The values of D_I found in this work are in good agreement with those found by Nemoto et al. confirming the prediction from the Borsali-Benmouna theory that D_I is only weakly dependent on the polymer molar mass differences between the two studies. There is also good agreement between the values of s found in this study and those found by Nemoto et al [30], indicating that the sedimentation friction coefficient too is only weakly dependent on the polymer molar mass differences.

The good agreement between the dynamic light scattering determined D_I and the ultracentrifuge determined D supports three conclusions. First that the ultra centrifugation theory for binary polymer solutions can be extended to the kinds of ternary polymer solution studied here. Second that the Borsali-Benmouna [3] theory adequately describes dynamic light scattering from these solutions, implying that thiophenol is a sufficiently equally good solvent for the two polymers. And thirdly that the diffusion coefficient obtained from the ultracentrifugation studies of such a solution is the interpenetration diffusion coefficient obtained from dynamic light scattering studies.

The values of D_I decreases as the temperature is lowered. This shows that phase separation could be induced by lowering the solution temperature. This result supports the Benmouna et al [4] theory of DLS from case A type ternary polymer solutions close to phase separation in which $q\xi$ was always less than unity. The correlation length critical exponent, n, for this system was found to be 0.60 ± 0.07.

6.2 PVME / PS / Thiophenol system.

The fact that the ternary solutions formed with PVME and polystyrene dissolved in thiophenol phase separated when subjected to strong centrifugal forces indicates that the solutions were indeed close to phase separation. This in turn leads one to conclude that thiophenol is not an equally good solvent for the polymers. Although it is tempting to assert that the solvent is of unequal quality for the two polymers, we have no direct evidence to support such a conclusion.

REFERENCES

1. M. R. Aven, C. Cohen, *Macromolecules* **23**, 476-486 (1990).

2. M. Benmouna, H. Benoit, Z. Akcasu, *Macromolecules* **20**, 1107-1112 (1987a).

3. M. Benmouna, H. Benoit, R. Borsali, M. Duval, *Macromolecules* **20**, 2620-2624 (1987b).

4. M. Benmouna, J. Seils, *Macromolecules* **26**, 668-678 (1993).

5. H. Benoit, M. Benmouna, *Macromolecules* **17**, 535 (1984).

6. B. J. Berne, R. Pecora, *Dynamic Light Scattering* (John Wiley and Sons, New York, 1976).

7. F. W. Billmeyer, *Textbook of Polymer Science* (John Wiley and Sons, New York, 1984).

8. R. Borsali, M. Duval, M. Benmouna, *Macromolecules* **22**, 816-821 (1989).

9. W. Brown, J. Fundin, *Macromolecules* **24**, 5171-5178 (1991).

10. W. Brown, *Dynamic Light Scattering, The Method and Some Applications* (Clarendon, Oxford, 1993), vol. 1.

11. C. H. Chervenka, *A Manual of Methods for the Analytical Ultracentrfuge* (Beckmann Instruments Inc., 1969).

12. B. Chu, *Laser Light Scattering* (Academic Press, INC., New York, 1974).

13. D. Clark, Masters Thesis, Massey University, New Zealand (1996).

14. Z. Cummins, E. Pike, *Photon Correlation and Light Beating Spectroscopy* (Plenum Press, New York, 1974).

15. Z. Cummins, E. Pike, *Photon Correlation Spectroscopy and Velocimetry* (Plenum Press, New York, 1977).

16. P. J. Daivis, Ph. D Thesis, Massey University, New Zealand (1989).

17. P. J. Daivis, D. N. Pinder, *Macromolecules* **26**, 3381-3390 (1993).

18. V. Degiorgio, M. Corti, M. Giglio, *Light Scattering in Liquids and Macromolecular Solutions* (Plenum Press, New York, 1980).

19. P. J. Flory, *Principles of Polymer Chemistry* (Cornell University Press., London, 1978).

20. H. Fujita, *Foundations of Ultracentrifugal Analysis* (John Wiley and Sons, New York, 1975).

21. T. Fukuda, M. Nagata, H. Inagaki, *Macromolecules* **17**, 548 (1984).

22. L. Giebel, R. Borsali, G. Meier, *Macromolecules* **23**, 4054-4060 (1990).

23. L. Giebel, M. Benmouna, R. Borsali, E. Fischer, *Macromolecules* **26**, 2433-2438 (1993).

24. J. J. Harvey, M. Sc. Thesis, Massey University, New Zealand (1995).

25. E. Jakeman, in *Photon Correlation and Light Beating Spectroscopy*(Plenum Press, New York, .

26. L. O. Kaddour, C. Strazielle, *Polymer* **28**, 459 (1987).

27. C. Konac, Z. Tuzar, J. Jakes, *Polymer* **31**, 1866 (1990).

28. Y. Luo, Ph. D Thesis, Massey University, New Zealand (1996).

29. N. Miyashita, M. Okada, T. Nose, *Polymer* **35**, 1038 (1994).

30. N. Nemoto, T. Inoue, Y. Makita, Y. Tsunashima, M. Kurata, *Macromolecules* **18**, 2516 (1985).

31. R. C. O'Driscoll, D. N. Pinder, *J. Phys. E: Sci. Instrum.* **13**, 192 (1980).

32. R. Pecora, *Dynamic Light Scattering* (Pienum Press, New York, 1985).

33. D. N. Pinder, D. Clark, P. Daivis, *Macromolecular Reports* **A31**, 1119-1126 (1994).

34. D. N. Pinder, Trends In Macromolecules Research, Research Trends, Kaithamukku, India, 1995),

35. D. N. Pinder, T. Ueleni, J. A. Lewis, *J. Molecular Structure* **in press.**, (1995).

36. Pinder, *Polymer* **5**, (1996).

37. P. Pusey, L. Vaughan, Specialist Periodical Reports of the Chemical Society, London, Light Scattering and Intensity Fluctuation Spectroscopy (1975).

38. P. N. Pusey, H. M. Fijnaut, A. Vrij, *J. Chem. Phys* **77**, 4270 (1982).

39. A. Robard, D. Patterson, G. Delmas, *Macromolecules* **10**, 706 (1977).

40. F. Roby, J. F. Joanny, *Macromolecules* **25**, 4612-4618

41. S. Saeki, S. Tsubotani, H. Kominami, M. Tsubokawa, *J. Poly. Sci.; Poly. Phys.* **24**, (1986).

42. J. Seils, M. Benmouna, *Macromolecules* **27**, 5043-5051 (1994).

43. M. Shibayama, H. Yang, R. S. Stein, C. C. Han, *Macromolecules* **18**, 2179 (1985).

44. C. S. Su, D. Patterson, *Macromolecules* **10**, 708 (1977).

45. Z. Sun, C. H. Wang, *Macromolecules* **27**, 5667-5673 (1994).

46. G. Wang, G. Fytas, D. Lilge, T. Dorfmuller, *Macromolecules* **14**, 1363 (1981).

47. H. Yamakawa, *Modern Theory of Polymer Solutions* (Harper and Row, New York, 1971).

48. K. Schatzel, *Quantum Opt.* **2**, 287-305 (1990)

Appendix. Publication

Comparision of diffusion coefficients obtained from ternary polymer solutions using dynamic light scattering and ultracentrifugation